Western Geotechnical Research Centre

Geotechnical Research Centre
Faculty of Engineering
The University of Western Ontario
Research Report GEOT-10-03

Expansion Of Cavities Embedded In Cohesionless Elastoplastic Half-Space And Subjected To Anisotropic Stress Fluid

H. El Naggar and M.H. El Naggar

The University of Western Ontario
Department of Civil and Environmental Engineering Faculty of Engineering Science

Expansion of cavities embedded in cohesionless elastoplastic half-space and subjected to anisotropic stress field

Hany El Naggar[1], Ph.D., P. Eng. and M. Hesham El Naggar[2], Ph.D., P. Eng.

[1]*Department of Civil Engineering – ALHOSN University, Abu Dhabi, UAE, email:* h.elnaggar@alhosnu.ae
[2]*Department of Civil & Environmental Engineering – University of Western Ontario, Canada, email:* helnaggar@eng.uwo.ca

ABSTRACT

Cavity expansion theories are employed in a wide range of geotechnical applications including interpretation of pressuremeter tests, evaluation of shaft capacity of piles, and pulling forces for horizontal directional drilling. Most of these theories assume infinite medium and isotropic stress field, which may not be justified for many applications. The main objectives of this paper are two folds: to investigate the effects of the free surface, stress gradient, and in-situ stress anisotropy on the displacements during the expansion phase of cavities embedded in dilatant sands; and to establish correction factors to account for these effects. The investigation was conducted using two-dimensional finite element analyses. It was found that the cavity expansion theory due to Yu and Houlsby (1991) can be used reliably for cases subjected to an initial isotropic stress and embedment depth to diameter ratio of 20 or higher. However, it becomes inaccurate for shallow embedment depth and/or stress anisotropy conditions. An analytical procedure to account for the effects of embedment and/or stress anisotropy was proposed. The applicability of the proposed procedure was demonstrated for a wide range of soil properties and geometrical configurations. The results obtained confirmed its ability to estimate the cavity pressures within 10% of the values obtained using FEA calculations.

Keywords: Cavity expansion, horizontal direction drilling, cohesionless material, SSI

1 INTRODUCTION

The cavity expansion theory was originally developed by Bishop et al. (1945) and Hill (1950) for application to metals. The theory was then applied to geomaterials (e.g. Chadwick, 1959; Gibson & Anderson, 1961) and has progressively advanced over the years (e.g. Vesic, 1972; Carter et al., 1986; Salgado et al. 1997).

The cavity expansion theories have been applied to a wide range of applications spanning from interpretation of pressuremeter tests (e.g. Gibson & Anderson, 1961; Palmer, 1972; Hughes et al., 1977; Houlsby and Withers, 1988) to piles (e.g. Randolph et al., 1979; El Naggar and Sakr, 2000). For such applications, the loading configuration of interest is perpendicular to the cavity plane and consequently the isotropic stress field assumption (i.e., the coefficient of lateral earth pressure, K_o =1) and zero stress-gradient is justifiable. The use of such theories for other applications such as the Horizontal Directional Drilling (HDD) and tunneling is emerging (e.g. Fernando and Moore, 2002; Yu and carter, 2002). However, the K_o=1 assumption for such applications is not justifiable as the loading configuration is in the cavity plane and thus the coefficient of lateral earth pressure is not always equal unity and the stress gradient would affect the soil behavior. In addition, these theories always presume an infinite medium and therefore the effect of the free ground surface (i.e., embedment depth) is always ignored.

The semi-analytical solution for expansion of cylindrical cavities in elasto-plastic dilatant soils developed by Yu and Houlsby (1991) considers the large strain effects, which is suitable for HDD applications that involve huge strains accompanying the upsizing of the cavity.

The main assumptions of the Yu and Houlsby (1991) solution are: 1) infinite medium; and 2) isotropic stress field everywhere (i.e., the coefficient of lateral earth pressure, K_o =1). As mentioned earlier, these assumptions are not justified for most HDD applications, and the effect of any deviation from these assumptions needs to be evaluated.

The main objectives of this paper are two folds: to investigate the effects of the free surface, stress gradient, and in-situ stress anisotropy (i.e. Ko≠ 1) on the displacements during the expansion phase of cavities embedded in dilatant sands; and to establish correction factors to account for these effects. In order to achieve these objectives, a finite element model was built using the software Plaxis. The finite element model was first verified for the case of infinite medium and isotropic stress field. The verified model was then used to perform an extensive parametric study in order to examine the effects of different influencing parameters of the HDD installation. The results obtained from the parametric study were used to establish correction factors to account for the coupled effects of the embedment depth and stress anisotropy.

2 CAVITY EXPANSION AND CONTRACTION THEORY

Yu and Houlsby (1991) used the Mohr-Coulomb yield criterion to derive an analytical solution for the expansion of a cylindrical cavity in a dilatant elasto-plastic soil medium. As this paper is devoted to the case of cohesionless soils (i.e., sand), the solution will be presented only for the case of pure cohesionless materials (i.e., c = 0). In this solution, the geometry of the problem is defined by the initial radius of the cavity, $a_{o,}$ the radius at the end of the expansion phase, a_1, and the external radius of the plastic zone at the end of the expansion phase d_1. Figure 1 shows the geometry of the expansion phase.

Soil properties used to characterize the soil behavior during the expansion phase are: the elastic modulus, E; Poisson's ratio, ν; angle of internal friction, ϕ; dilation angle, ψ; and the initial pressure P_o, which is a function of the overburden pressure above the point of interest.

The following are functions of the soil properties used in the derivation of the analytical solution in order to abbreviate the mathematical manipulation.

$$G = \frac{E}{2(1+\upsilon)} \quad [1]$$

$$\alpha = \frac{(1+\sin\phi)}{(1-\sin\phi)} \quad [2]$$

$$\beta = \frac{(1+\sin\psi)}{(1-\sin\psi)} \quad [3]$$

$$\delta = \frac{(\alpha-1)P_o}{2(1+\alpha)G} \quad [4]$$

$$\gamma = \frac{\alpha(\beta+1)}{(\alpha-1)\beta} \quad [5]$$

$$\eta = \exp\left(\frac{(\beta+1)(1-2\nu)(1+\nu)P_o}{E\beta}\right) \quad [6]$$

$$\mu = \frac{1+\beta}{\alpha-1} \quad [7]$$

$$\iota = \frac{E}{2(1-\upsilon^2)\ P_o} \quad [8]$$

Where,

G is the shear modulus of the soil, α is a function of friction angle, β is a function of dilation angle, δ is a function of soil properties and the initial state of stress, P_o, while γ, η, μ, and ι are functions of the selected soil properties.

2.1 Expansion phase (loading case):

2.1.1 Elastic conditions

The radial cavity pressure, P (the additional pressure, i.e. $P = P_t - P_o$), at a given radius, a, during the elastic stage of expansion can be calculated by (Yu, et al 1991):

$$P = 2G\delta + P_O \qquad [9]$$

The radius, a, is then related to the initial cavity radius a_o by (Yu, et al 1991):

$$\frac{a}{a_o} = 1 + \frac{(P - P_o)}{2G} \qquad [10]$$

2.1.2 Elastic-plastic conditions

During the elastic-plastic stage, the radius of the interface between the elastic and plastic zones is given by:

$$\frac{d_1}{a} = R^{\frac{\alpha}{(\alpha-1)}} \qquad [11]$$

Where d_1 is the radius of the plastic zone, R is the cavity pressure ratio given by Eq.13, and a is given by:

$$\frac{a}{a_o} = \left[\frac{R^{-\gamma}}{(1-\delta)^{\frac{(\beta+1)}{\beta}} - (\frac{\gamma}{\eta})\, A_1(R,\xi)} \right]^{\frac{\beta}{(\beta+1)}} \qquad [12]$$

where

$$R = \frac{(1+\alpha)P}{2\alpha P_o} \qquad [13]$$

and

$$A_1(R,\ \zeta) = \sum_{n=0}^{\infty} A_n^1 \qquad [14]$$

in which

$$A_n^1 = \begin{cases} \dfrac{y^n \ln x}{n!} & \text{if} \quad n=\gamma \\ \dfrac{y^n (x^{(n-\gamma)} - 1)}{n!(n-\gamma)} & \text{otherwise} \end{cases} \qquad [15]$$

where $A_1(R,\zeta)$ is an infinite series; $A_n^{\ 1}$ is the general term of the series, x and y are variables representing (R,ζ) and n is the number of terms (Yu and Houlsby 1991).

3 NUMERICAL MODEL

This section has two objectives: to verify the capabilities of the finite element model to capture the response of the tackled problem, which involves high level of expansion reaching up to 150% of the original radius (i.e., a/ao=1.5); and to investigate the effect of deviation from the assumptions of the analytical solution on its predictions. The first objective is achieved by examining a finite element model (Mesh 1) that has the same geometric and loading conditions as that of the analytical solution (i.e. infinite medium and constant isotropic stress field everywhere). The second objective will be accomplished in two steps: a) to validate the finite element model (Mesh 2) that will be used later throughout the study; b) to utilize Mesh 2 to perform a parametric study to investigate the effect of embedment depth (i.e. free surface condition) on the accuracy of the analytical solution. For the latter case, a mesh with a very high burial depth, cover to diameter ratio, C/D = 40 (Mesh 2) was used to minimize the free surface effects during the validation process as discussed later.

3.1 Finite Element Mesh and Its Verification

The fifteen-nodded cubic strain triangular finite element included in the element library of the FE package PLAXIS (Brinkgreve, 2002) was used to simulate the expansion process of a plane strain cylindrical cavity subjected to radial internal pressure. Taking advantage of symmetry for both meshes, only the right half of the problem was modeled. The lateral and bottom boundaries were placed about 40 times the cavity diameter to simulate the infinite medium. The size of the model was selected such that the artificial boundaries and boundary conditions would not affect the ground stresses around the

cavity. The problem geometry and the FE Mesh 1 are shown in Figure 2; whereas, Figure 3 shows Mesh 2.

The Mohr-Coulomb failure criterion (i.e. elasto-plastic stress-strain relationship) was used as the constitutive model for the ground. The criterion assumes a linear elastic soil behavior up to the defined Mohr-Coulomb failure surface. If the failure surface is reached, the soil yields, with corresponding stress redistribution to maintain equilibrium, up to the point where the stress conditions in the soil zones do not violate the yield surface and become again acceptable under the failure criterion. The material was modeled as purely frictional soil (i.e. c = 0) with the following properties: Young's modulus, E = 50 MPa, Poisson's ratio, ν = 0.35, angle of friction, ϕ= 35º and angle of dilatation, ψ = 5º.

3.1.1 Validation Phase

Mesh 1

As stated earlier, this mesh has the same geometric and loading conditions as that of the analytical solution, i.e., infinite medium and constant isotropic stress field everywhere. The cavity was assumed to expand to a/ao=1.1, a/ao=1.3, and a/ao=1.5. For all cases, the distribution of the radial stresses around the internal boundary of the cavity was constant (i.e. no change along the circumference) as shown in Figure 4. This is expected since the internal prescribed displacements and the vertical and horizontal stresses are equal; K_o= 1). Figure 5 illustrates and compares the relationship between radial cavity pressures normalized by initial soil pressure P/P_o versus cavity radius normalized by the initial cavity radius a/a_o calculated from the FE to that obtained from the analytical solution. As

it can be seen from Figure 5, there is a great agreement between the FE predictions and the closed form solution (CFS) results. This demonstrates the ability of the mesh to capture the response of the tackled problem and the suitability of the mesh size. Therefore, it can be used to study the effect of stress anisotropy on the predictions of the CFS.

Mesh 2

This mesh will be used in the subsequent section to study the effect of the embedment depth. To verify this mesh, a cavity embedded at cover to diameter ratio, C/D = 40 was tested. The cavity was expanded to a/ao=1.1, a/ao=1.3, and a/ao=1.5. The loading conditions of this mesh involve a stress gradient that increases linearly with depth. Thus, the distribution of the radial stresses around the internal boundary of the cavity varied with depth with lower values of resistance at the cavity crown (location of lower initial stresses) and larger values at its invert. Figure 6 shows sample stress distribution for the cavity as it approaches a/ao=1.5 (the same trend was found to hold for all cases). The variation of stresses in Figure 6 is limited due to the high embedment ratio in this case (C/D = 40), which would not be the case for low embedment ratios such as C/D = 10, 5, or 2.5.

Figure 7 compares the relationship between radial cavity pressures normalized by initial soil pressure P/P_o versus cavity radius normalized by the initial cavity radius a/a_o calculated from the FE to that obtained from the CFS. The CFS results are within less than 2% from the FE predictions. This implies that at high burial depths, the effect of the

assumption of infinite depth (i.e. neglecting the effect of free surface) on the CFS results is negligible.

4 EFFECT OF THE FREE SURFACE AND THE STRESS GRADIENT

An extensive parametric study was conducted to investigate the effect of the embedment depth (i.e. the free surface situation) on the predicted response from the CFS by comparing its results to that obtained from the FE analysis.

In the parametric study, a cavity expansion of up to 150% (i.e., the expanded diameter is 1.5 times the original diameter) was considered. Different analyses considered expansion ratios, a/ao = 1.1, 1.2, 1.3, 1.4 and 1.5, which means upsizing ratios of 10, 20, 30, 40 and 50%, respectively. These upsizing ratios cover the practical range for the majority of HDD installations. Three levels of embedment were considered, C/D = 40 and 20, C/D = 10 and 7.5 and C/D = 5 and 2.5, which represents high, medium and low embedment, respectively.

Figures 8, 9 and 10 display the radial cavity pressures normalized by the initial soil pressure, P/Po, versus the cavity radius normalized by the initial cavity radius, a/ao, for loose sand for burial depths that vary from C/D = 40 to C/D = 2.5. It can be noted from Figures 8 to 10 that the relationship between cavity pressure and its radius during the expansion phase is nonlinear. For high embedment depths (C/D = 40, 20), the CFS predictions are close enough to that obtained from the FE calculations as shown in Figure 8 (within less than 3% difference for the lowest case of C/D = 20). Thus, it can be noted

that up to embedment depth of C/D = 20, the CFS can predict the behaviour with reasonable accuracy.

As the embedment depth decreases, the free surface effects are clearly manifested as can be seen from Figure 9, which presents the results for the medium embedment case (C/D = 10, 7.5). In this case, the difference between the CFS and FE results is 20% for expansion ratio, a/ao = 1.3 and C/D = 10, and 27% for the same expansion ratio with C/D = 7.5. Moreover, the difference reaches up to 26% for a/ao = 1.5 with C/D = 10, and 30% for a/ao = 1.5 with C/D = 7.5.

For the case of low embedment depths of C/D = 5 or 2.5, the disagreement is even worse as it can be noted from Figure 10, the magnitude of difference escalates to 40% for expansion ratio, a/ao = 1.5 with C/D = 5, and 54% for a/ao = 1.5 with C/D = 2.5.

The results of the parametric study demonstrated that the CFS overestimates the required cavity pressure to expand the cavity during the expansion phase. This is due to the increased resistance implied by the CFS assumption that the stress field is constant to an infinite distance in every direction. On the other hand, in the simulated real case (i.e. the FE model), the stress diminishes towards the surface. Thus, the resistance to cavity expansion is less and the pressure required to expand the cavity is less. This is more prevalent for C/D ratios $\leq$ 10 or less.

5 EFFECT OF THE IN-SITU STRESS ANISOTROPY

This section examines the effect of the in-situ stress anisotropy (i.e. $K_o \neq 1$) on the displacements during expansion of cavities embedded in dilatant sands. The calculated results of FE analysis were compared to the CFS predicted response in order to evaluate

the magnitude of approximations induced by the CFS assumptions for such cases (i.e. K_o<1).

In order to separate the effect of in-situ stress anisotropy from the influence of the embedment depth and stress gradient, very high embedment depth was utilized (C/D=40). In the study, four different values of coefficient of lateral earth pressure at rest, K_o, were considered (K_o=1.0, 0.8, 0.6 and 0.4). The expansion was assumed to increase up to 150% with upsizing ratios of 10, 20, 30, 40 and 50%, respectively.

The results for the in-situ isotropic stress state case (K_o= 1.0) are shown in Figure 11a. As can be noted from the figure, the FE predictions agree well with those obtained from the closed form solution at all expansion levels. This agreement becomes less favorable for cases involving in-situ stress anisotropy as shown in Figures 11b, 11c and 11d. Figure 11b shows that for the case of Ko= 0.8, the CFS overestimates the cavity pressures during the expansion phase by up to 11%, whereas for K_o= 0.6 and 0.4, the CFS overestimates the cavity pressures by up to 30% and by 58%, respectively, as shown in Figures 11c and. This trend is expected and is related to the early onset of yielding as the confining stresses decrease for cases with K_o<1.0. Thus, a smaller amount of cavity pressure results in the same cavity displacement.

6 CORRECTION FACTOR FOR THE EMBEDMENT DEPTH

The results showed that the closed form solution for cavity expansion can be used reliably for up to an embedment depth, C/D = 20. However, as the embedment depth decreases, the stress gradient affects its accuracy substantially. The CFS overestimates the cavity pressures by up to 54% for a/ao = 1.5 with C/D = 2.5. Table 1 summarizes

some of the selected results of the parametric study and the magnitude of error associated with each case. These differences can have significant implications when evaluating the forces associated with HDD installations and the selection of the necessary equipment, which may impact the economic feasibility of the HDD installation. It is therefore necessary to correct the predicted pressure values to account for effects of embedment. A nonlinear regression analysis was performed using the results of the finite element analysis to determine the best fit and the coefficients for the nonlinear quadratic equation for the correction factor R_D which is dependent on the independent variables C/D and a/ao. Consequently, the following expression for the correction factor was obtained:

$$R_d = \frac{-2.14}{(C/D)} - \frac{0.51}{(a/a_o)} + \frac{0.45}{(C/D \times a/a_o)} + \frac{2.32}{(C/D)^2} + \frac{0.51}{(a/a_o)^2} + 1.14 \qquad [16]$$

where,

$\frac{a}{a_o}$ = is ratio of the expanded radius to the original radius

$\frac{C}{D}$ = is the ratio of the depth to the springline to the diameter

6.1 Verification of the obtained correction factor

The aim of this section is to verify the applicability of the obtained correction factor for several cases covering a practical range of soil and geometric parameters. The range covered include angle of internal friction, ϕ, ranging from 30º to 40º; dilation angle, ψ, ranging from 0º to 15º; and Poisson's ratio, ν, from 0.25 to 0.45.

Several cases were considered in the verification process. A sample of these cases for medium and low embedment ratios (the ones shown to have high deviation) is presented here to showcase the applicability of the proposed correction factor. Three soil conditions were considered for each embedment depth, with two ψ values for each soil condition. The soil conditions considered are loose, medium, and dense sand.

Figures 12 and 13 present some of the corrected cases for C/D = 10 and 5, representing medium and low embedment, respectively. As shown in Figure 12, the predictions of the corrected solution are within less than 5% from the results of the FEA for the loose and medium dense sand cases and within 8% at most for the dense sand case. These values contrast with up to 29% without the correction factor. For C/D = 5, the results of the corrected solution are within less than 5% from the results of the FEA for the loose and medium sand cases and within less than 8% for the dense sand case, which represent a significant improvement over the discrepancy of up to 45% without the correction factor.

These results of the verification process showed that the results of the closed form solution employing the correction factor are within less than of 10% of the FE calculations. Thus, the proposed correction factor can dampened the difference between the CFS and the FE from up to 45% to 10% or less.

7 CORRECTION FACTOR FOR THE IN-SITU STRESS ANISOTROPY

The semi-analytical solution for expansion of cylindrical cavities in elasto-plastic dilatant soils by Yu and Houlsby (1991) was developed assuming isotropic stress field conditions, i.e., the coefficient of lateral earth pressure at rest, K_o=1.0. As mentioned earlier, such assumption may be justifiable for some applications such as the interpretation of pressuremeter tests and evaluation of shaft capacity of tapered piles. However, this

assumption is not justifiable for HDD application and may introduce an error more than 50% due to the K_o effect alone (apart from the C/D effect). In order to account for this effect, a correction factor was obtained utilizing a nonlinear regression analysis of the results obtained from the parametric study. The results were obtained for seven different values of coefficient of lateral earth pressure at rest, K_o (1.0, 0.9, 0.8, 0.7, 0.6, 0.5 and 0.4). The proposed correction factor depends on the coefficient of lateral earth pressure at rest, Ko; the cover to depth ratio, C/D; and the ratio of the current radius to the original radius, a/ao, as shown in the following formula.

$$R_k = (K_o - 1)(0.5 - \frac{1.08}{C/D} + \frac{0.57}{a/a_o}) - 0.24(K_o^2 - 1) \qquad [17]$$

R_k should be added to the coefficient R_d to get an overall correction factor that accounts for both the coefficient of lateral earth pressure at rest and the embedment depth.

8 CORRECTION FOR THE COUPLED EFFECT OF THE EMBEDMENT DEPTH AND IN-SITU STRESS ANISOTROPY

It is common that an HDD installation encounters soil conditions that involve both initial stress anisotropy and low burial depth. For example, pipes with diameters ranging from 300mm to 600 mm installed just blow the frost depth of around 2 to 3 meters would result in an embedment depth ratio (C/D) ranging from 5 to 10. These shallow C/D ratios alone can result in more than 40% overestimation. Coupling this with the effect of initial stress anisotropy, the overestimation can reach 90% or more, i.e. nearly double the cavity pressure value. This vast overestimation can have significant impact on the selection of

the equipment needed for the installation, which may adversely impact the economic feasibility of the project.

8.1 Procedure for calculating cavity expansion pressure

A procedure is proposed herein to correct the predictions of the CFS accounting for the coupled effects of initial stress anisotropy and free surface, as follows:

i) Calculate the initial stress P_o, which corresponds to the initial cavity with radius a_o.

ii) Calculate the parameters given by Equations 1 o 9, which are functions of soil properties.

iii) For a given value of the additional cavity pressure, P, less than $P_1 = (\alpha - 1)P_o/(\alpha + 1)$, the response remains in the elastic stage of expansion and the corresponding radius a can be calculated by Equation 10.

iv) For an additional cavity pressure, P, exceeding the limiting pressure P_1, the cavity pressure ratio R is calculated from Equation 13.

v) Equations 14 and 15 are used to evaluate A_1 – only a few terms are sufficient.

vi) Evaluate a/a_o from Equation 12, and from that the cavity pressure can be determined.

vii) For the cases with initial isotropic stress, i.e. K_o=1, the calculated cavity pressure ratio is corrected to account for the burial depth using the correction factor, R_d, given by Equation 16, viz:

$$\left(\frac{P_t}{P_o}\right)_{\text{Corrected}} = \left(\frac{P_t}{P_o}\right)_{\text{CFS}} \times R_d$$

viii) For cases involving initial stress anisotropy, i.e. K_o<1, the ocalculated cavity pressure ratio is corrected to account for both stress anisotropy and burial depth using the

the correction factor, R_{dk}, which is the summation of the two correction factors, R_d and R_k, i.e.,

$$\left(\frac{P_t}{P_o}\right)_{Corrected} = \left(\frac{P_t}{P_o}\right)_{CFS} \times R_{dk}$$

where,

$$R_{dk} = R_d + R_k$$

8.2 Evaluation of the proposed procedure

8.2.1 Soil strength characterization

The shear strength of sand depends on a number of factors, including the nature of loading (triaxial or plane strain), drainage conditions (drained or undrained), initial state (loose or dense), and the type of fabric (fine or coarse). The angle of dilatancy, ψ, of sand is affected by the relative density and the effective stress (Bolton, 1986). Depending on the sand mineralogy (quartz or feldspar), typical values of the angle of internal frication of sands range from 30º to 40º, whereas the typical values of ψ range from 0º to 15º.

8.2.2 Results of the evaluation process

The applicability of the proposed correction procedure was evaluated for several cases covering a practical range of soils, ranging from loose to dense sand; geometric parameters ranging from C/D = 2.5 to 20; and initial stress anisotropy with K_o ranging from 0.4 to 0.8. Table 2 summarizes the geometric information and soil properties of the considered cases.

Figure 14 presents some of the corrected cases for low embedment ratios (i.e., C/D = 2.5 and 5). The results of the CFS adjusted using the correction factors are within 7% of the FE calculations. Thus, the proposed correction factor reduces the difference between the CFS and the FE from up to 86% to less than 7%. Figure 15 presents some of the corrected results for medium and high embedment ratios (i.e., C/D = 10 and 20). The corrected CFS results are within less than 9% of that of the FE calculations.

9 CONCLUSIONS

The results obtained in this study demonstrated that the closed form solution for cavity expansion due to Yu and Houlsby (1991) can be used reliably for cases subjected to an initial isotropic stress and embedment depth, C/D = 20 or higher. However, as the embedment depth decreases, the free surface condition affects its accuracy. The study also showed that the stress anisotropy conditions can lead to a significant overestimation of the cavity pressure calculated from the closed form solution. This overestimation can have significant implications when evaluating the forces associated with HDD installations and sizing the required equipment for the operation. It is therefore necessary to correct the predicted pressure values to account for effects of embedment and stress anisotropy. An analytical procedure to account for the effects of embedment and/or stress anisotropy was proposed. The proposed procedure was evaluated against several cases covering a wide spectrum of soil properties and geometrical configurations. The results obtained using the proposed method confirmed its usefulness and its ability to estimate the cavity pressures within 10% of the values obtained using FEA calculations.

REFERENCES

Bishop, R.F., Hill, R. and Mott, N.F. 1945. Theory of indentation and hardness tests. Proc. Phys. Soc., 57: 147

Bolton, M.D. 1986. The strength and dilatancy of sands. *Geotechnique* 36(1): 65-78.

Carter, J.P., Booker, J.R. and Yeung, S.K. 1986. Cavity expansion in cohesive frictional soils. *Geotechnique* 36(3): 349-358

Chadwick, P. 1959. The quasi-static expansion of a spherical cavity in metals and ideal soils. Q. J. Mech. Appl. Math., 12: 52-71.

El Naggar, M.H. and Sakr, M. 2000. Evaluation of axial performance of tapered piles from centrifuge tests. Canadian Geotechnical Journal, 37(6): 1295-1308.

Fernando, V. and Moore, I.D. 2002. Use of cavity expansion theory to predict ground displacement during pipe bursting. Proc. of Pipelines 2002, ASCE, Cleveland, OH, July, 11pp

Gibson, R. E. & Anderson, W. F. 1961. In situ measurement of soil properties with the pressuremeter. Civil Engineering Public Works Rev. 56: 615-618.

Hill, R. 1950. The mathematical theory of plasticity. Oxford University Press, London.

Houlsby, G.T. and Withers, N.J. 1988. Analysis of the cone pressuremeter test in clay. *Geotechnique*, 38: 573-587.

Hughes, J. M. O., Wrath, C. P. & Windle, D.1977. Pressuremeter tests in sands. *Geotechnique*, 27(4): 455-477.

Palmer, A. C. (1972). Undrained plane-strain expansion of a cylindrical cavity in clay: a simple interpretation of the pressuremeter test. *Geotechnique* 22(3): 451-457.

Randolph, M. F., Carter, J. P. & Wrath, C. P.1979. Driven piles in clay--the effects of installation and subsequent consolidation. *Geotechnique* 29(4): 361-393.

Salgado, R., Mitchell, J.K., and Jamiolkowski, M. 1997. Cavity expansion and penetration resistance in sand. ASCE, Journal of Geotechnical and Geoenvironmental Engineering, 123(4): 344-354.

Vesic, A. S. 1972. Expansion of cavities in infinite soil mass. J. Soil Mech. Fdns Div. ASCE 98, SM3, 265-290.

Yu, H.S and Houlsby, G.T. 1991. Finite cavity expansion in dilatant soils: loading analysis. *Geotechnique*, Vol. 41:173-183.

Yu, H.S. and Houlsby, G.T. 1995. A large strain analytical solution for cavity contraction in dilatant soils. International Journal for Numerical and Analytical Methods in Geomechanics, Vol. 19:793-811.

Yu H.S. and Rowe R.K.1999, Plasticity solutions for soil behaviour around contracting cavities and tunnels. International Journal for Numerical and Analytical Methods in Geomechanics, Vol. 23: 1245-1279.

Yu H.S. and Carter, J.P. 2002. Rigorous similarity solutions for cavity expansion in cohesive-frictional soils. International Journal of Geomechanics, Vol. 2(3).

Table 1. Selected results of the parametric study.

C/D	Closed form Solution		Finite Element Analysis		Error %
	a/a_o	P/P_o	a/a_o	P/P_o	
2.5	1	0	1	0	0.00%
2.5	1.03	7.70	1.03	6.13	25.61%
2.5	1.06	10.30	1.06	8.44	22.08%
2.5	1.09	11.80	1.09	9.35	26.25%
2.5	1.20	15.17	1.20	11.12	36.48%
2.5	1.30	16.98	1.30	11.82	43.68%
2.5	1.40	18.20	1.40	12.66	43.72%
2.5	1.50	19.25	1.50	12.49	54.06%
5	1	0	1	0	0.00%
5	1.02	4.97	1.02	4.51	10.21%
5	1.06	7.62	1.06	6.48	17.64%
5	1.09	9.05	1.09	7.31	23.85%
5	1.20	11.57	1.20	8.92	29.69%
5	1.30	12.95	1.30	9.81	32.05%
5	1.40	13.92	1.40	10.15	37.18%
5	1.50	14.67	1.50	10.45	40.41%
7.5	1	0	1	0	0.00%
7.5	1.02	4.27	1.02	4.15	3.01%
7.5	1.05	5.97	1.05	5.60	6.62%
7.5	1.09	7.77	1.09	6.78	14.56%
7.5	1.20	9.87	1.20	7.89	25.16%
7.5	1.30	11.07	1.30	8.69	27.37%
7.5	1.40	11.90	1.40	9.05	31.43%
7.5	1.50	12.50	1.50	9.61	30.06%
10	1	0	1	0.000	0.00%
10	1.01	3.45	1.01	3.40	1.48%
10	1.04	5.37	1.04	5.09	5.47%
10	1.09	6.88	1.09	6.46	6.43%
10	1.20	8.80	1.20	7.39	19.03%
10	1.30	9.90	1.30	8.23	20.22%
10	1.40	10.65	1.40	8.66	23.04%
10	1.50	11.19	1.50	8.88	26.06%
20	1	0.00	1	0.000	0.00%
20	1.02	2.97	1.02	2.89	2.63%
20	1.03	3.77	1.03	3.73	0.94%
20	1.09	5.28	1.09	5.26	0.43%
20	1.20	6.74	1.20	6.65	1.34%
20	1.30	7.55	1.30	7.39	2.16%
20	1.40	8.07	1.40	7.93	1.72%
20	1.50	8.47	1.50	8.22	3.09%

Table 2: geometric information and soil properties of the considered cases

Case #	C/D	Soil Properties					Max. Error %	
		K_o	ϕ^o	ψ^o	υ	*E (MPa)*	***Before Correction***	***After Correction***
1	2.5	0.4	40	15	0.4	90	76.34%	6.08%
2	2.5	0.4	40	0	0.4	90	76.42%	6.17%
3	5	0.4	40	0	0.4	60	86.21%	4.02%
4	5	0.5	35	0	0.3	20	69.17%	2.26%
5	7.5	0.5	33	10	0.3	60	61.11%	1.69%
6	7.5	0.66	38	10	0.3	90	52.06%	6.87%
7	10	0.8	30	15	0.35	20	27.36%	1.95%
8	10	0.8	30	0	0.35	20	24.03%	1.88%
9	10	0.8	40	15	0.35	80	37.66%	8.95%
10	10	0.8	40	0	0.35	80	41.64%	9.5%
11	20	0.6	35	10	0.35	40	34.32%	1.72%
12	20	0.6	35	0	0.35	40	42.41%	8.32%

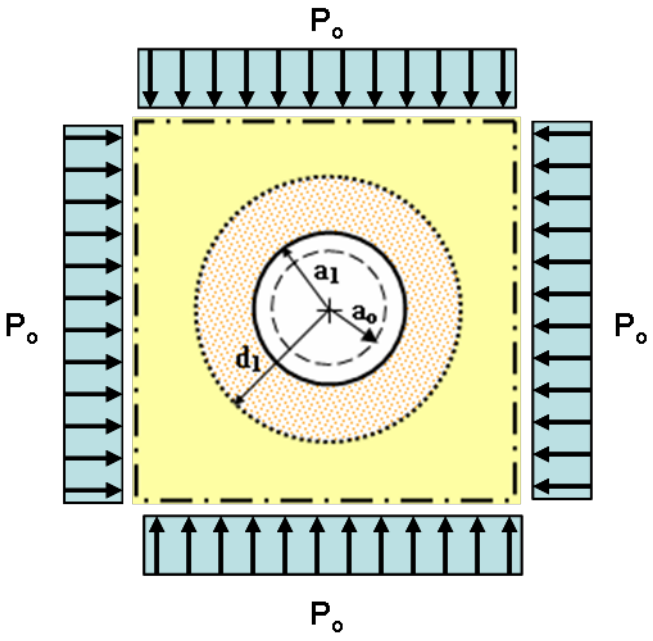

Figure 1. Geometry of the expansion phase.

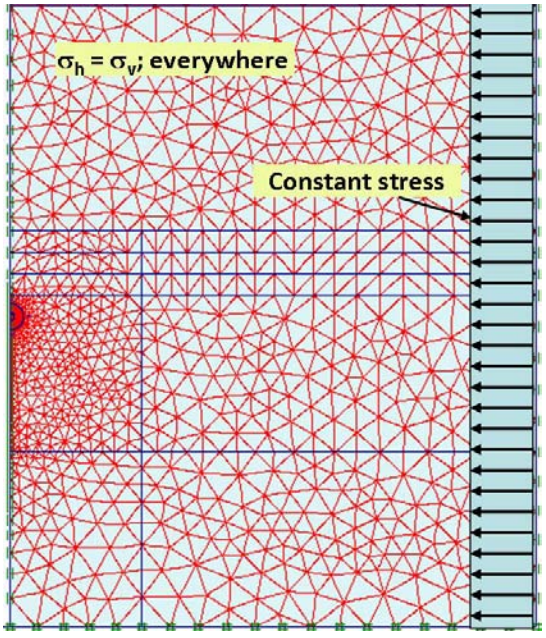

Figure 2. Problem geometry and the FE Mesh 1

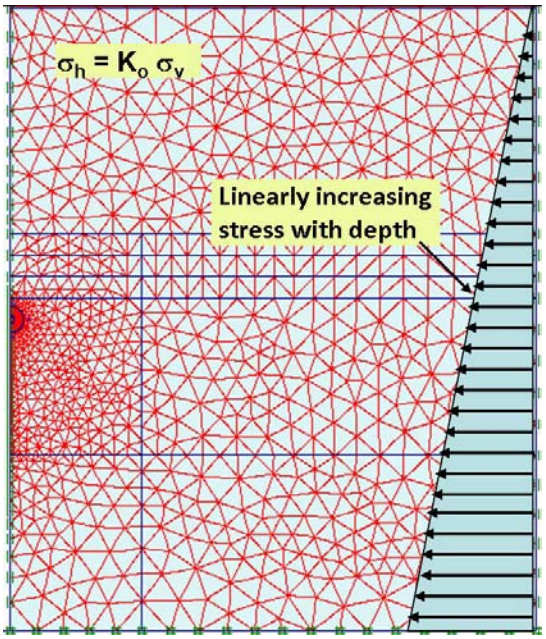

Figure 3. Problem geometry and the FE Mesh 2

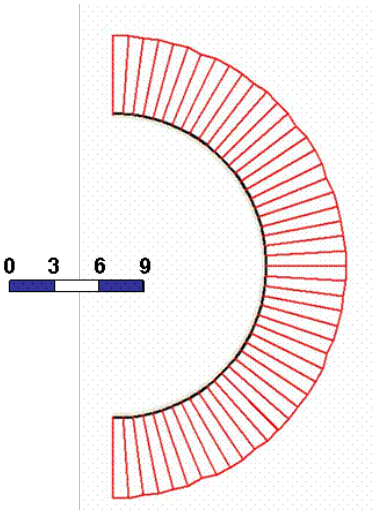

Figure 4. Radial cavity pressure normalized by initial soil pressure, P/Po

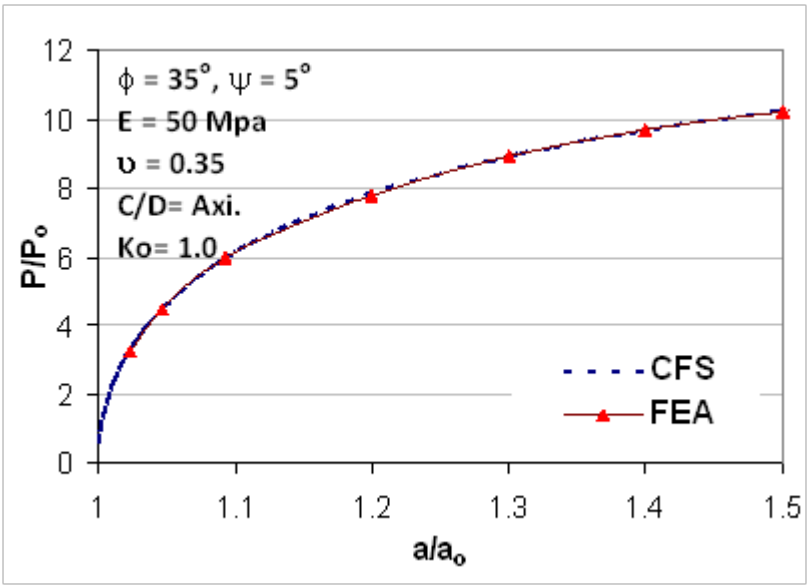

Figure 5. Radial cavity pressure normalized by initial soil pressure, P/Po, versus the cavity radius normalized by the initial cavity radius, a/ao, for medium sand.

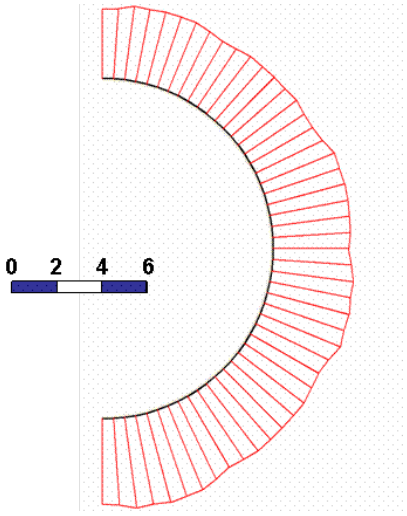

Figure 6. Radial cavity pressure normalized by initial soil pressure, P/Po

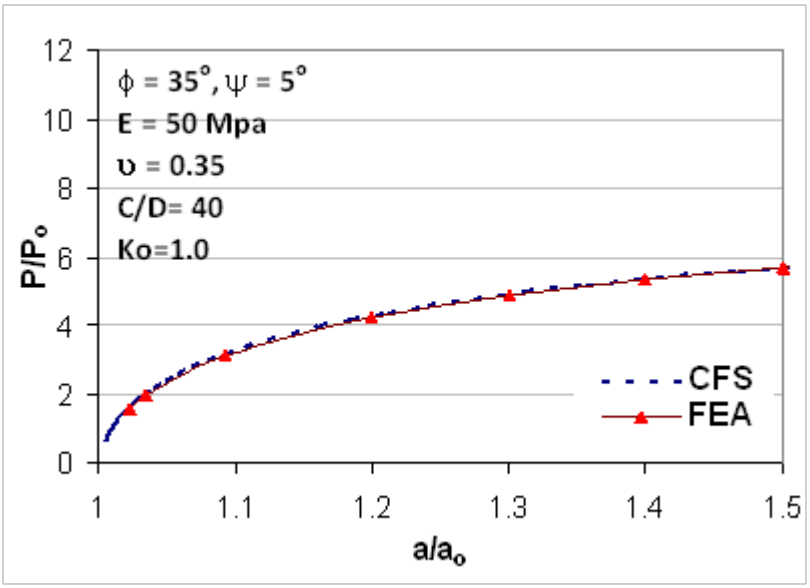

Figure 7. Radial cavity pressure normalized by initial soil pressure, P/P_o, versus the cavity radius normalized by the initial cavity radius, a/a_o, for C/D=40.

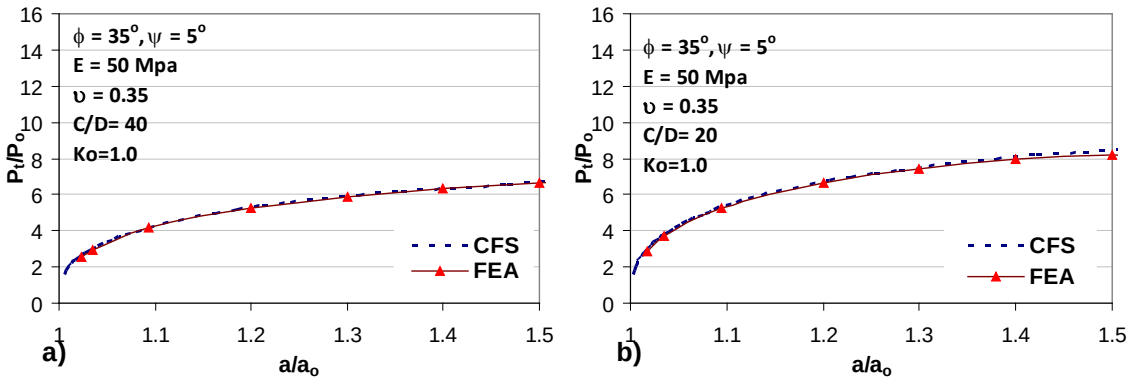

Figure 8. Radial cavity pressure normalized by initial soil pressure, P/Po, versus the cavity radius normalized by the initial cavity radius, a/ao, for: a) C/D=40, b) C/D=20.

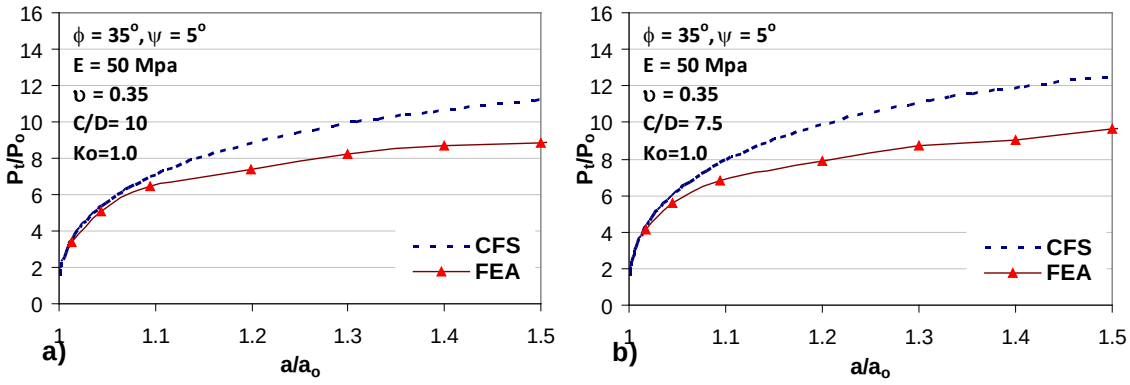

Figure 9. Radial cavity pressure normalized by initial soil pressure, P/Po, versus the cavity radius normalized by the initial cavity radius, a/ao, for: a) C/D=10, b) C/D=7.5.

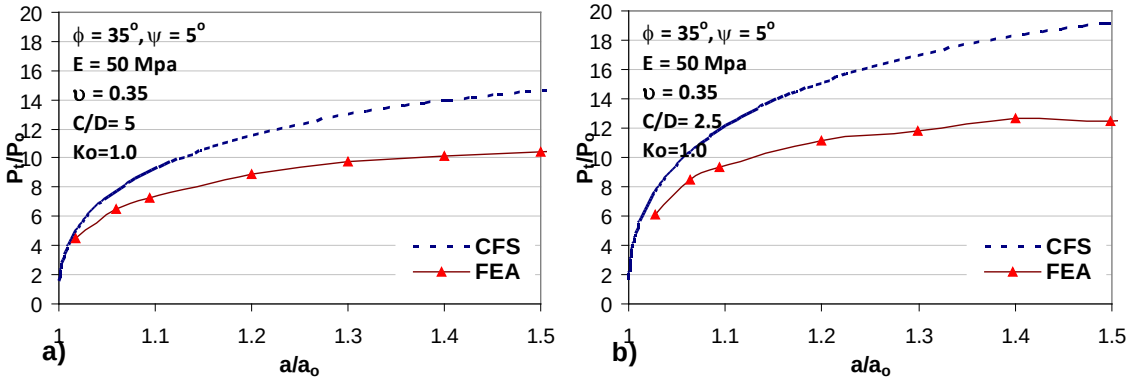

Figure 10. Radial cavity pressure normalized by initial soil pressure, P/Po, versus the cavity radius normalized by the initial cavity radius, a/ao, for: a) C/D=5, b) C/D=2.5.

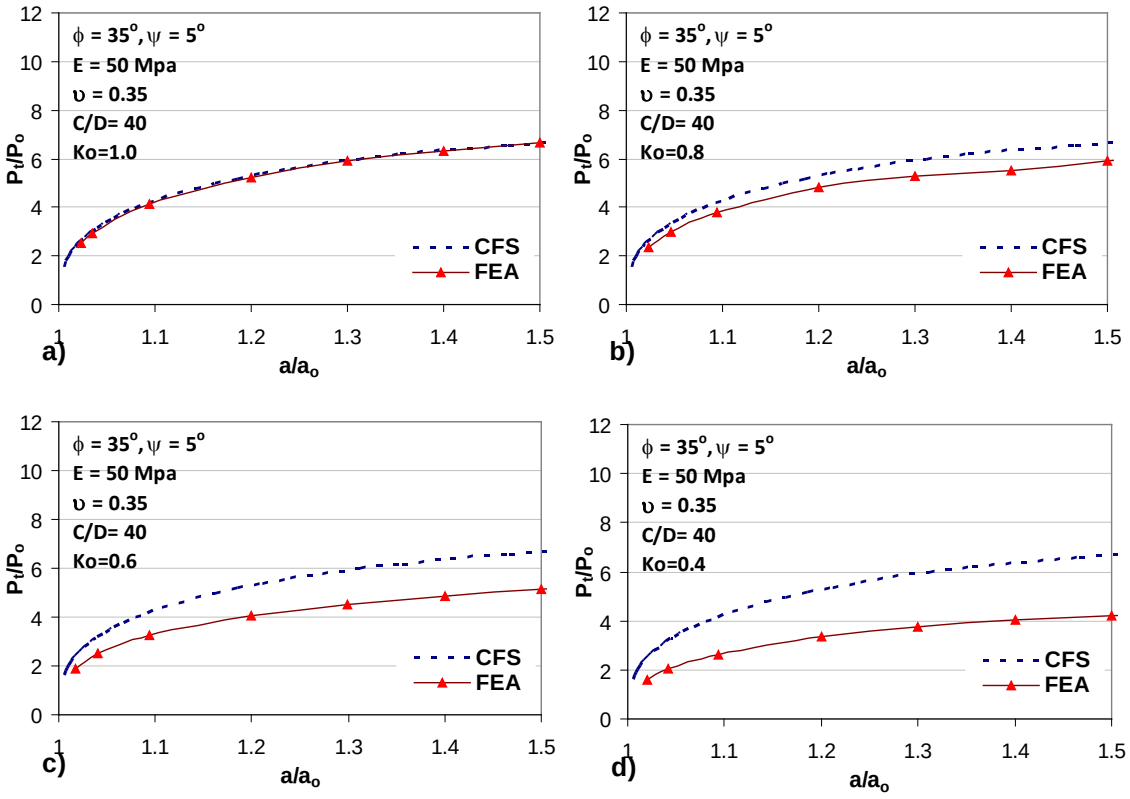

Figure 11. Radial cavity pressure normalized by initial soil pressure, P/Po, versus the cavity radius normalized by the initial cavity radius, a/ao, for: a)Ko =1.0, b) Ko =0.8, c) Ko =0.6, d) Ko =0.4.

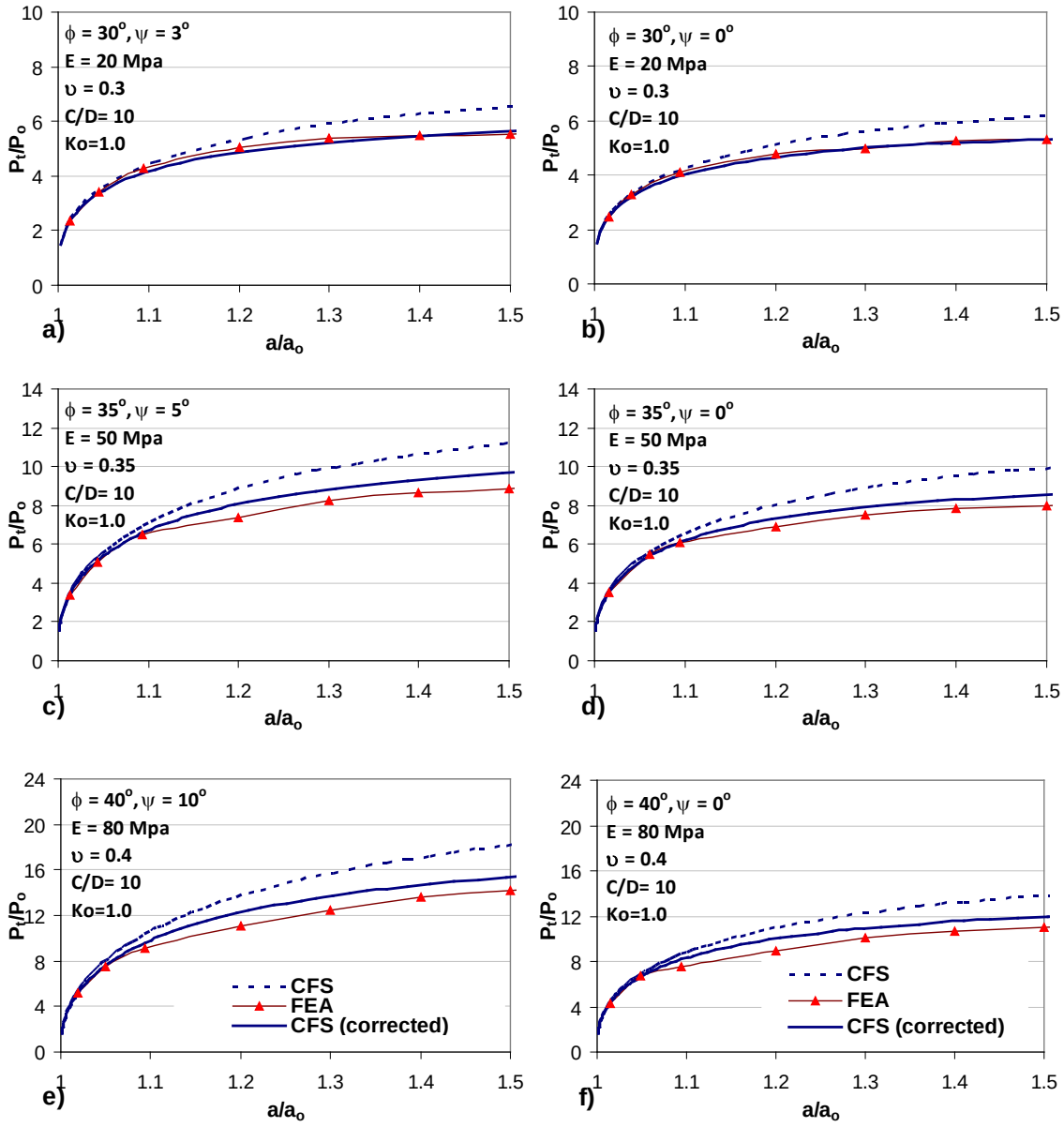

Figure 12. Radial cavity pressure normalized by initial soil pressure, P/Po, versus the cavity radius normalized by the initial cavity radius, a/ao, for sample of some corrected cases for C/D=10 and Ko=1.0.

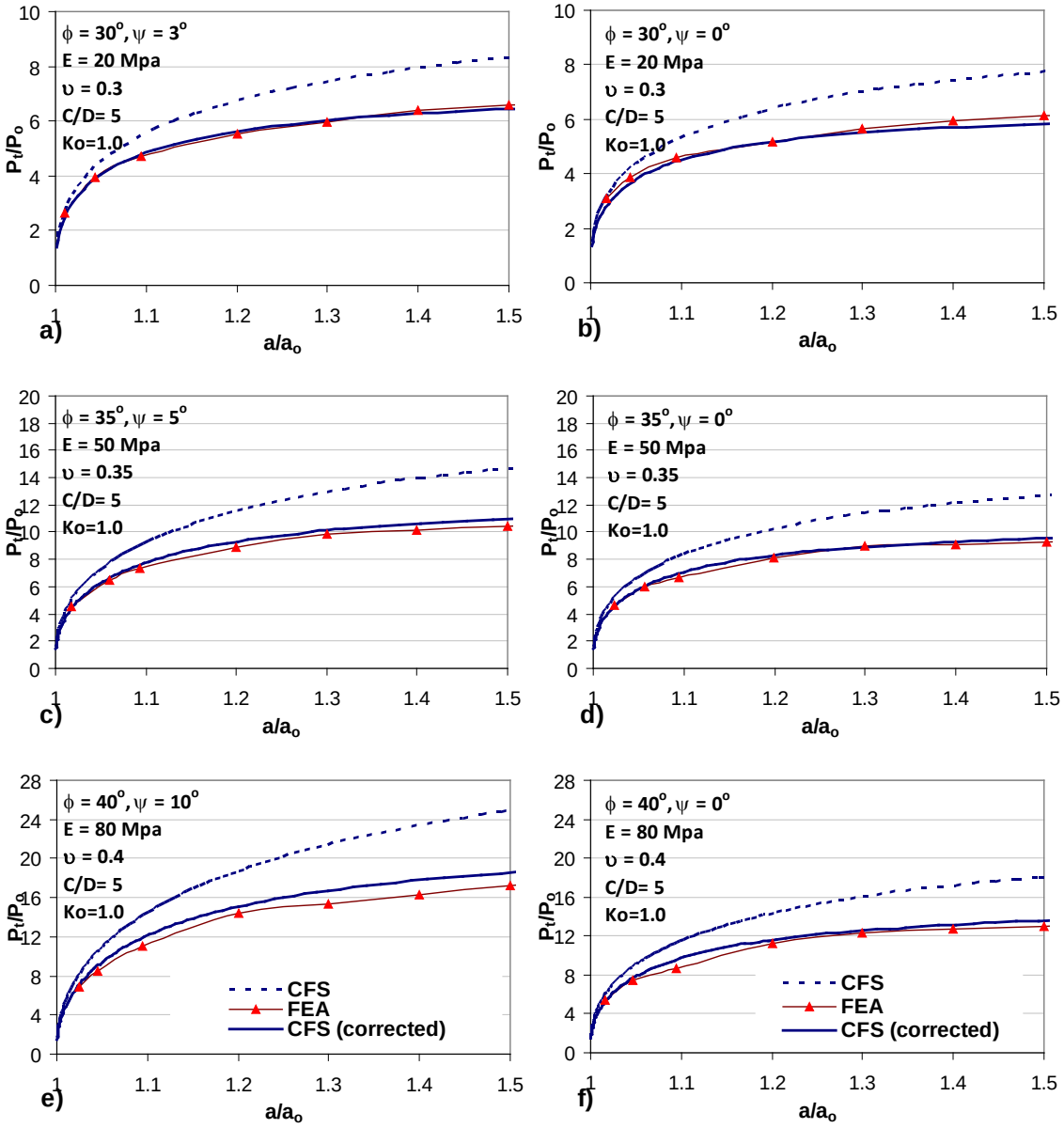

Figure 13. Radial cavity pressure normalized by initial soil pressure, P/Po, versus the cavity radius normalized by the initial cavity radius, a/ao, for sample of some corrected cases for C/D=5 and Ko=1.0.

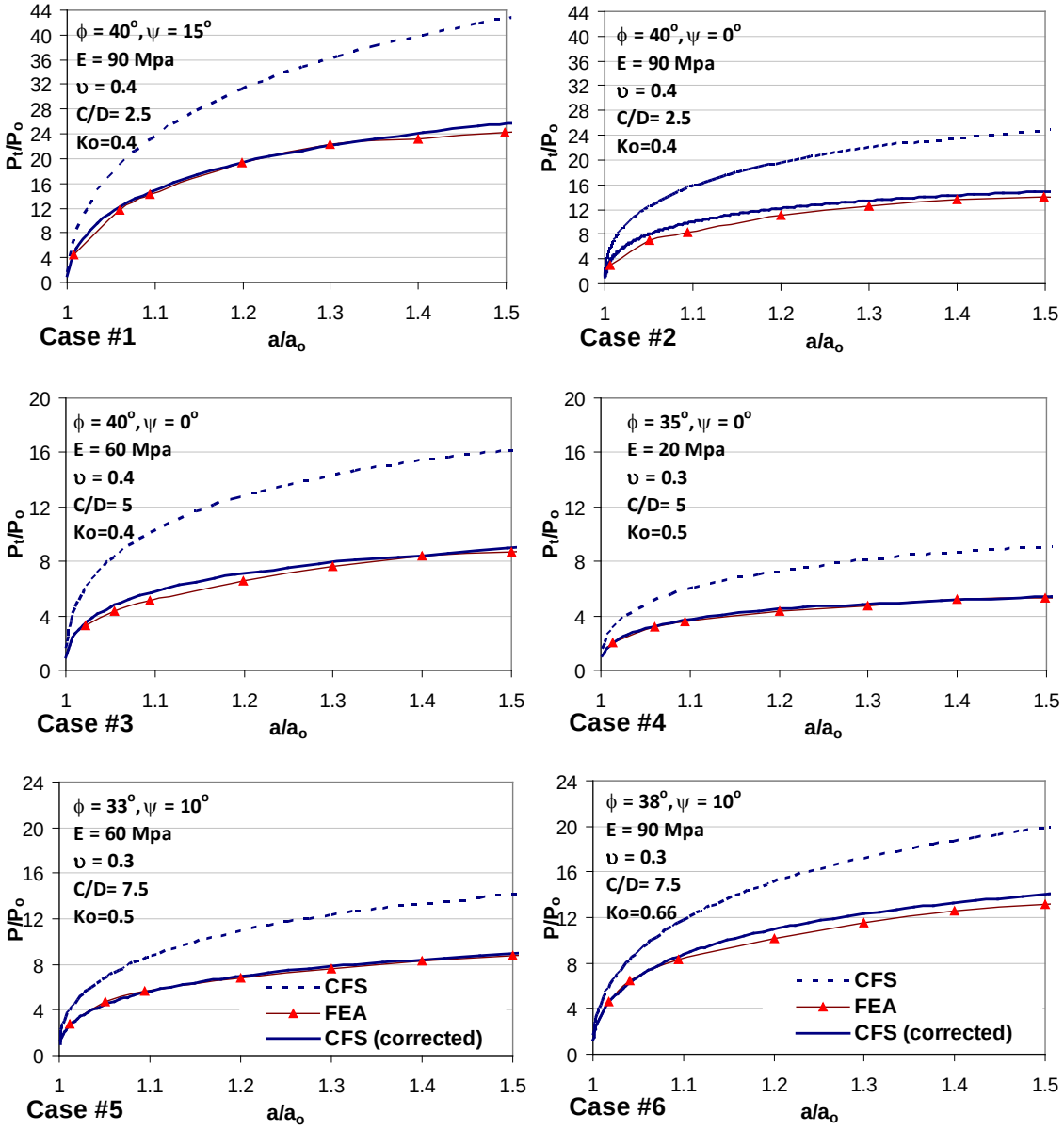

Figure 14. Radial cavity pressure normalized by initial soil pressure, P/Po, versus the cavity radius normalized by the initial cavity radius, a/ao, for sample of some corrected cases for combined effect of C/D and K_o low embedment.

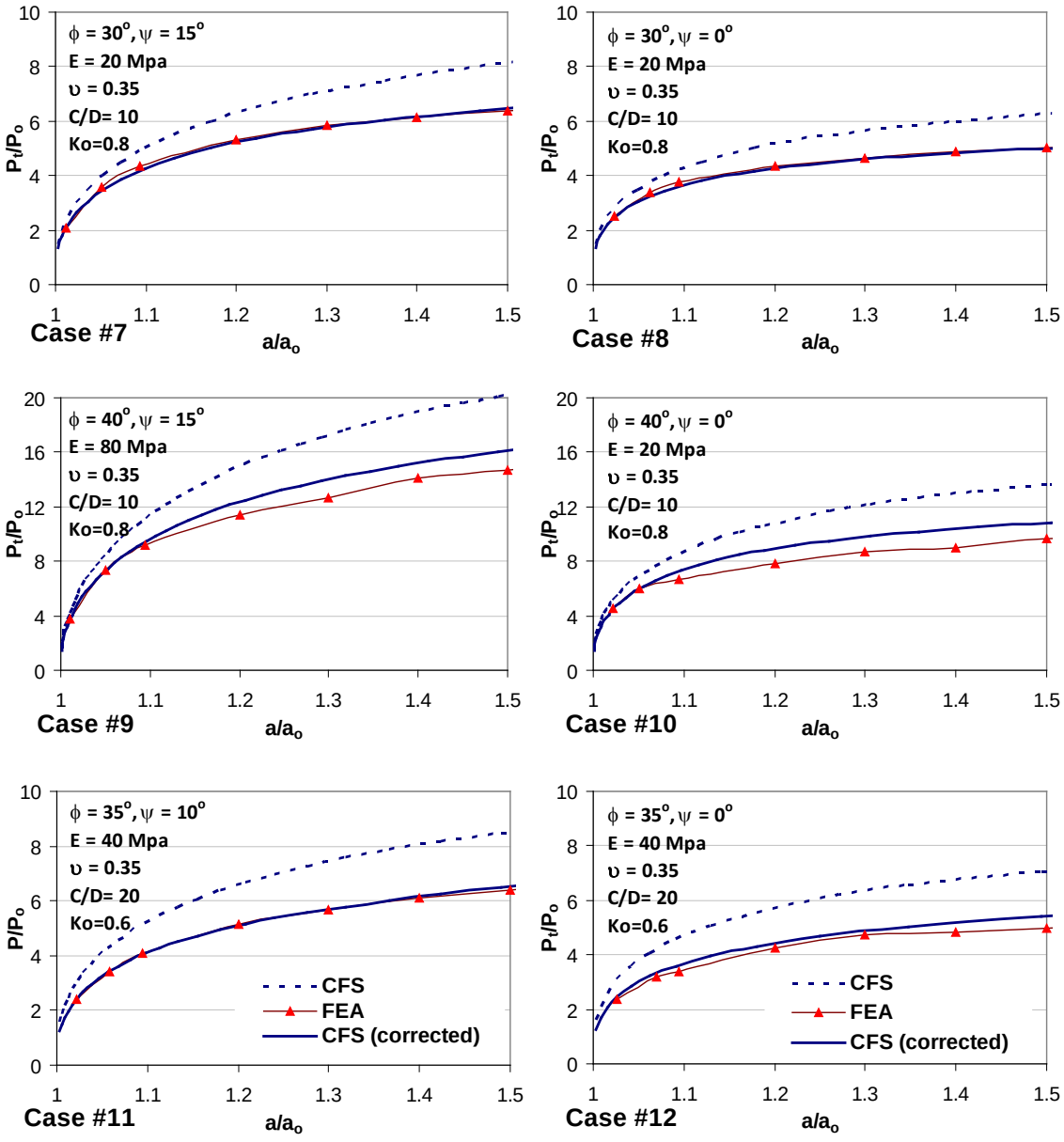

Figure 15. Radial cavity pressure normalized by initial soil pressure, P/Po, versus the cavity radius normalized by the initial cavity radius, a/ao, for sample of some corrected cases for combined effect of C/D and K_o medium and embedment.

Expansion of cavities embedded in cohesionless elastoplastic half-space and subjected to anisotropic stress field

Hany El Naggar[1], Ph.D., P. Eng. and M. Hesham El Naggar[2], Ph.D., P. Eng.

[1]*Department of Civil Engineering – ALHOSN University, Abu Dhabi, UAE, email:* h.elnaggar@alhosnu.ae
[2]*Department of Civil & Environmental Engineering – University of Western Ontario, Canada, email:* helnaggar@eng.uwo.ca

ABSTRACT

Cavity expansion theories are employed in a wide range of geotechnical applications including interpretation of pressuremeter tests, evaluation of shaft capacity of piles, and pulling forces for horizontal directional drilling. Most of these theories assume infinite medium and isotropic stress field, which may not be justified for many applications. The main objectives of this paper are two folds: to investigate the effects of the free surface, stress gradient, and in-situ stress anisotropy on the displacements during the expansion phase of cavities embedded in dilatant sands; and to establish correction factors to account for these effects. The investigation was conducted using two-dimensional finite element analyses. It was found that the cavity expansion theory due to Yu and Houlsby (1991) can be used reliably for cases subjected to an initial isotropic stress and embedment depth to diameter ratio of 20 or higher. However, it becomes inaccurate for shallow embedment depth and/or stress anisotropy conditions. An analytical procedure to account for the effects of embedment and/or stress anisotropy was proposed. The applicability of the proposed procedure was demonstrated for a wide range of soil properties and geometrical configurations. The results obtained confirmed its ability to estimate the cavity pressures within 10% of the values obtained using FEA calculations.

Keywords: Cavity expansion, horizontal direction drilling, cohesionless material, SSI

1 INTRODUCTION

The cavity expansion theory was originally developed by Bishop et al. (1945) and Hill (1950) for application to metals. The theory was then applied to geomaterials (e.g. Chadwick, 1959; Gibson & Anderson, 1961) and has progressively advanced over the years (e.g. Vesic, 1972; Carter et al., 1986; Salgado et al. 1997).

The cavity expansion theories have been applied to a wide range of applications spanning from interpretation of pressuremeter tests (e.g. Gibson & Anderson, 1961; Palmer, 1972; Hughes et al., 1977; Houlsby and Withers, 1988) to piles (e.g. Randolph et al., 1979; El Naggar and Sakr, 2000). For such applications, the loading configuration of interest is perpendicular to the cavity plane and consequently the isotropic stress field assumption (i.e., the coefficient of lateral earth pressure, K_o =1) and zero stress-gradient is justifiable. The use of such theories for other applications such as the Horizontal Directional Drilling (HDD) and tunneling is emerging (e.g. Fernando and Moore, 2002; Yu and carter, 2002). However, the K_o=1 assumption for such applications is not justifiable as the loading configuration is in the cavity plane and thus the coefficient of lateral earth pressure is not always equal unity and the stress gradient would affect the soil behavior. In addition, these theories always presume an infinite medium and therefore the effect of the free ground surface (i.e., embedment depth) is always ignored.

The semi-analytical solution for expansion of cylindrical cavities in elasto-plastic dilatant soils developed by Yu and Houlsby (1991) considers the large strain effects, which is suitable for HDD applications that involve huge strains accompanying the upsizing of the cavity.

The main assumptions of the Yu and Houlsby (1991) solution are: 1) infinite medium; and 2) isotropic stress field everywhere (i.e., the coefficient of lateral earth pressure, K_o =1). As mentioned earlier, these assumptions are not justified for most HDD applications, and the effect of any deviation from these assumptions needs to be evaluated.

The main objectives of this paper are two folds: to investigate the effects of the free surface, stress gradient, and in-situ stress anisotropy (i.e. Ko≠ 1) on the displacements during the expansion phase of cavities embedded in dilatant sands; and to establish correction factors to account for these effects. In order to achieve these objectives, a finite element model was built using the software Plaxis. The finite element model was first verified for the case of infinite medium and isotropic stress field. The verified model was then used to perform an extensive parametric study in order to examine the effects of different influencing parameters of the HDD installation. The results obtained from the parametric study were used to establish correction factors to account for the coupled effects of the embedment depth and stress anisotropy.

2 CAVITY EXPANSION AND CONTRACTION THEORY

Yu and Houlsby (1991) used the Mohr-Coulomb yield criterion to derive an analytical solution for the expansion of a cylindrical cavity in a dilatant elasto-plastic soil medium. As this paper is devoted to the case of cohesionless soils (i.e., sand), the solution will be presented only for the case of pure cohesionless materials (i.e., c = 0). In this solution, the geometry of the problem is defined by the initial radius of the cavity, $a_{o,}$ the radius at the end of the expansion phase, a_1, and the external radius of the plastic zone at the end of the expansion phase d_1. Figure 1 shows the geometry of the expansion phase.

Soil properties used to characterize the soil behavior during the expansion phase are: the elastic modulus, E; Poisson's ratio, ν; angle of internal friction, ϕ; dilation angle, ψ; and the initial pressure P_o, which is a function of the overburden pressure above the point of interest.

The following are functions of the soil properties used in the derivation of the analytical solution in order to abbreviate the mathematical manipulation.

$$G = \frac{E}{2(1+\upsilon)} \quad [1]$$

$$\alpha = \frac{(1+\sin\phi)}{(1-\sin\phi)} \quad [2]$$

$$\beta = \frac{(1+\sin\psi)}{(1-\sin\psi)} \quad [3]$$

$$\delta = \frac{(\alpha-1)P_o}{2(1+\alpha)G} \quad [4]$$

$$\gamma = \frac{\alpha(\beta+1)}{(\alpha-1)\beta} \quad [5]$$

$$\eta = \exp\left(\frac{(\beta+1)(1-2\nu)(1+\nu)P_o}{E\beta}\right) \quad [6]$$

$$\mu = \frac{1+\beta}{\alpha-1} \quad [7]$$

$$\iota = \frac{E}{2(1-\upsilon^2)\ P_o} \quad [8]$$

Where,

G is the shear modulus of the soil, α is a function of friction angle, β is a function of dilation angle, δ is a function of soil properties and the initial state of stress, P_o, while γ, η, μ, and ι are functions of the selected soil properties.

2.1 Expansion phase (loading case):

2.1.1 Elastic conditions

The radial cavity pressure, P (the additional pressure, i.e. $P = P_t - P_o$), at a given radius, a, during the elastic stage of expansion can be calculated by (Yu, et al 1991):

$$P = 2G\delta + P_O \qquad [9]$$

The radius, a, is then related to the initial cavity radius a_o by (Yu, et al 1991):

$$\frac{a}{a_o} = 1 + \frac{(P - P_o)}{2G} \qquad [10]$$

2.1.2 Elastic-plastic conditions

During the elastic-plastic stage, the radius of the interface between the elastic and plastic zones is given by:

$$\frac{d_1}{a} = R^{\frac{\alpha}{(\alpha-1)}} \qquad [11]$$

Where d_1 is the radius of the plastic zone, R is the cavity pressure ratio given by Eq.13, and a is given by:

$$\frac{a}{a_o} = \left[\frac{R^{-\gamma}}{(1-\delta)^{\frac{(\beta+1)}{\beta}} - (\frac{\gamma}{\eta})\, A_1(R,\xi)} \right]^{\frac{\beta}{(\beta+1)}} \qquad [12]$$

where

$$R = \frac{(1+\alpha)P}{2\alpha P_o} \qquad [13]$$

and

$$A_1(R,\ \zeta) = \sum_{n=0}^{\infty} A_n^1 \qquad [14]$$

in which

$$A_n^1 = \begin{cases} \dfrac{y^n \ln x}{n!} & \text{if} \quad n=\gamma \\ \dfrac{y^n (x^{(n-\gamma)} - 1)}{n!(n-\gamma)} & \text{otherwise} \end{cases} \qquad [15]$$

where $A_1(R,\zeta)$ is an infinite series; $A_n^{\ 1}$ is the general term of the series, x and y are variables representing (R,ζ) and n is the number of terms (Yu and Houlsby 1991).

3 NUMERICAL MODEL

This section has two objectives: to verify the capabilities of the finite element model to capture the response of the tackled problem, which involves high level of expansion reaching up to 150% of the original radius (i.e., a/ao=1.5); and to investigate the effect of deviation from the assumptions of the analytical solution on its predictions. The first objective is achieved by examining a finite element model (Mesh 1) that has the same geometric and loading conditions as that of the analytical solution (i.e. infinite medium and constant isotropic stress field everywhere). The second objective will be accomplished in two steps: a) to validate the finite element model (Mesh 2) that will be used later throughout the study; b) to utilize Mesh 2 to perform a parametric study to investigate the effect of embedment depth (i.e. free surface condition) on the accuracy of the analytical solution. For the latter case, a mesh with a very high burial depth, cover to diameter ratio, C/D = 40 (Mesh 2) was used to minimize the free surface effects during the validation process as discussed later.

3.1 Finite Element Mesh and Its Verification

The fifteen-nodded cubic strain triangular finite element included in the element library of the FE package PLAXIS (Brinkgreve, 2002) was used to simulate the expansion process of a plane strain cylindrical cavity subjected to radial internal pressure. Taking advantage of symmetry for both meshes, only the right half of the problem was modeled. The lateral and bottom boundaries were placed about 40 times the cavity diameter to simulate the infinite medium. The size of the model was selected such that the artificial boundaries and boundary conditions would not affect the ground stresses around the

cavity. The problem geometry and the FE Mesh 1 are shown in Figure 2; whereas, Figure 3 shows Mesh 2.

The Mohr-Coulomb failure criterion (i.e. elasto-plastic stress-strain relationship) was used as the constitutive model for the ground. The criterion assumes a linear elastic soil behavior up to the defined Mohr-Coulomb failure surface. If the failure surface is reached, the soil yields, with corresponding stress redistribution to maintain equilibrium, up to the point where the stress conditions in the soil zones do not violate the yield surface and become again acceptable under the failure criterion. The material was modeled as purely frictional soil (i.e. c = 0) with the following properties: Young's modulus, E = 50 MPa, Poisson's ratio, ν = 0.35, angle of friction, ϕ= 35º and angle of dilatation, ψ = 5º.

3.1.1 Validation Phase

Mesh 1

As stated earlier, this mesh has the same geometric and loading conditions as that of the analytical solution, i.e., infinite medium and constant isotropic stress field everywhere. The cavity was assumed to expand to a/ao=1.1, a/ao=1.3, and a/ao=1.5. For all cases, the distribution of the radial stresses around the internal boundary of the cavity was constant (i.e. no change along the circumference) as shown in Figure 4. This is expected since the internal prescribed displacements and the vertical and horizontal stresses are equal; K_o= 1). Figure 5 illustrates and compares the relationship between radial cavity pressures normalized by initial soil pressure P/P_o versus cavity radius normalized by the initial cavity radius a/a_o calculated from the FE to that obtained from the analytical solution. As

it can be seen from Figure 5, there is a great agreement between the FE predictions and the closed form solution (CFS) results. This demonstrates the ability of the mesh to capture the response of the tackled problem and the suitability of the mesh size. Therefore, it can be used to study the effect of stress anisotropy on the predictions of the CFS.

Mesh 2

This mesh will be used in the subsequent section to study the effect of the embedment depth. To verify this mesh, a cavity embedded at cover to diameter ratio, C/D = 40 was tested. The cavity was expanded to a/ao=1.1, a/ao=1.3, and a/ao=1.5. The loading conditions of this mesh involve a stress gradient that increases linearly with depth. Thus, the distribution of the radial stresses around the internal boundary of the cavity varied with depth with lower values of resistance at the cavity crown (location of lower initial stresses) and larger values at its invert. Figure 6 shows sample stress distribution for the cavity as it approaches a/ao=1.5 (the same trend was found to hold for all cases). The variation of stresses in Figure 6 is limited due to the high embedment ratio in this case (C/D = 40), which would not be the case for low embedment ratios such as C/D = 10, 5, or 2.5.

Figure 7 compares the relationship between radial cavity pressures normalized by initial soil pressure P/P_o versus cavity radius normalized by the initial cavity radius a/a_o calculated from the FE to that obtained from the CFS. The CFS results are within less than 2% from the FE predictions. This implies that at high burial depths, the effect of the

assumption of infinite depth (i.e. neglecting the effect of free surface) on the CFS results is negligible.

4 EFFECT OF THE FREE SURFACE AND THE STRESS GRADIENT

An extensive parametric study was conducted to investigate the effect of the embedment depth (i.e. the free surface situation) on the predicted response from the CFS by comparing its results to that obtained from the FE analysis.

In the parametric study, a cavity expansion of up to 150% (i.e., the expanded diameter is 1.5 times the original diameter) was considered. Different analyses considered expansion ratios, a/ao = 1.1, 1.2, 1.3, 1.4 and 1.5, which means upsizing ratios of 10, 20, 30, 40 and 50%, respectively. These upsizing ratios cover the practical range for the majority of HDD installations. Three levels of embedment were considered, C/D = 40 and 20, C/D = 10 and 7.5 and C/D = 5 and 2.5, which represents high, medium and low embedment, respectively.

Figures 8, 9 and 10 display the radial cavity pressures normalized by the initial soil pressure, P/Po, versus the cavity radius normalized by the initial cavity radius, a/ao, for loose sand for burial depths that vary from C/D = 40 to C/D = 2.5. It can be noted from Figures 8 to 10 that the relationship between cavity pressure and its radius during the expansion phase is nonlinear. For high embedment depths (C/D = 40, 20), the CFS predictions are close enough to that obtained from the FE calculations as shown in Figure 8 (within less than 3% difference for the lowest case of C/D = 20). Thus, it can be noted

that up to embedment depth of C/D = 20, the CFS can predict the behaviour with reasonable accuracy.

As the embedment depth decreases, the free surface effects are clearly manifested as can be seen from Figure 9, which presents the results for the medium embedment case (C/D = 10, 7.5). In this case, the difference between the CFS and FE results is 20% for expansion ratio, a/ao = 1.3 and C/D = 10, and 27% for the same expansion ratio with C/D = 7.5. Moreover, the difference reaches up to 26% for a/ao = 1.5 with C/D = 10, and 30% for a/ao = 1.5 with C/D = 7.5.

For the case of low embedment depths of C/D = 5 or 2.5, the disagreement is even worse as it can be noted from Figure 10, the magnitude of difference escalates to 40% for expansion ratio, a/ao = 1.5 with C/D = 5, and 54% for a/ao = 1.5 with C/D = 2.5.

The results of the parametric study demonstrated that the CFS overestimates the required cavity pressure to expand the cavity during the expansion phase. This is due to the increased resistance implied by the CFS assumption that the stress field is constant to an infinite distance in every direction. On the other hand, in the simulated real case (i.e. the FE model), the stress diminishes towards the surface. Thus, the resistance to cavity expansion is less and the pressure required to expand the cavity is less. This is more prevalent for C/D ratios $\leq$ 10 or less.

5 EFFECT OF THE IN-SITU STRESS ANISOTROPY

This section examines the effect of the in-situ stress anisotropy (i.e. $K_o \neq 1$) on the displacements during expansion of cavities embedded in dilatant sands. The calculated results of FE analysis were compared to the CFS predicted response in order to evaluate

the magnitude of approximations induced by the CFS assumptions for such cases (i.e. K_o<1).

In order to separate the effect of in-situ stress anisotropy from the influence of the embedment depth and stress gradient, very high embedment depth was utilized (C/D=40). In the study, four different values of coefficient of lateral earth pressure at rest, K_o, were considered (K_o=1.0, 0.8, 0.6 and 0.4). The expansion was assumed to increase up to 150% with upsizing ratios of 10, 20, 30, 40 and 50%, respectively.

The results for the in-situ isotropic stress state case (K_o= 1.0) are shown in Figure 11a. As can be noted from the figure, the FE predictions agree well with those obtained from the closed form solution at all expansion levels. This agreement becomes less favorable for cases involving in-situ stress anisotropy as shown in Figures 11b, 11c and 11d. Figure 11b shows that for the case of Ko= 0.8, the CFS overestimates the cavity pressures during the expansion phase by up to 11%, whereas for K_o= 0.6 and 0.4, the CFS overestimates the cavity pressures by up to 30% and by 58%, respectively, as shown in Figures 11c and. This trend is expected and is related to the early onset of yielding as the confining stresses decrease for cases with K_o<1.0. Thus, a smaller amount of cavity pressure results in the same cavity displacement.

6 CORRECTION FACTOR FOR THE EMBEDMENT DEPTH

The results showed that the closed form solution for cavity expansion can be used reliably for up to an embedment depth, C/D = 20. However, as the embedment depth decreases, the stress gradient affects its accuracy substantially. The CFS overestimates the cavity pressures by up to 54% for a/ao = 1.5 with C/D = 2.5. Table 1 summarizes

some of the selected results of the parametric study and the magnitude of error associated with each case. These differences can have significant implications when evaluating the forces associated with HDD installations and the selection of the necessary equipment, which may impact the economic feasibility of the HDD installation. It is therefore necessary to correct the predicted pressure values to account for effects of embedment. A nonlinear regression analysis was performed using the results of the finite element analysis to determine the best fit and the coefficients for the nonlinear quadratic equation for the correction factor R_D which is dependent on the independent variables C/D and a/ao. Consequently, the following expression for the correction factor was obtained:

$$R_d = \frac{-2.14}{(C/D)} - \frac{0.51}{(a/a_o)} + \frac{0.45}{(C/D \times a/a_o)} + \frac{2.32}{(C/D)^2} + \frac{0.51}{(a/a_o)^2} + 1.14 \qquad [16]$$

where,

$\frac{a}{a_o}$ = is ratio of the expanded radius to the original radius

$\frac{C}{D}$ = is the ratio of the depth to the springline to the diameter

6.1 Verification of the obtained correction factor

The aim of this section is to verify the applicability of the obtained correction factor for several cases covering a practical range of soil and geometric parameters. The range covered include angle of internal friction, ϕ, ranging from 30º to 40º; dilation angle, ψ, ranging from 0º to 15º; and Poisson's ratio, ν, from 0.25 to 0.45.

Several cases were considered in the verification process. A sample of these cases for medium and low embedment ratios (the ones shown to have high deviation) is presented here to showcase the applicability of the proposed correction factor. Three soil conditions were considered for each embedment depth, with two ψ values for each soil condition. The soil conditions considered are loose, medium, and dense sand.

Figures 12 and 13 present some of the corrected cases for C/D = 10 and 5, representing medium and low embedment, respectively. As shown in Figure 12, the predictions of the corrected solution are within less than 5% from the results of the FEA for the loose and medium dense sand cases and within 8% at most for the dense sand case. These values contrast with up to 29% without the correction factor. For C/D = 5, the results of the corrected solution are within less than 5% from the results of the FEA for the loose and medium sand cases and within less than 8% for the dense sand case, which represent a significant improvement over the discrepancy of up to 45% without the correction factor.

These results of the verification process showed that the results of the closed form solution employing the correction factor are within less than of 10% of the FE calculations. Thus, the proposed correction factor can dampened the difference between the CFS and the FE from up to 45% to 10% or less.

7 CORRECTION FACTOR FOR THE IN-SITU STRESS ANISOTROPY

The semi-analytical solution for expansion of cylindrical cavities in elasto-plastic dilatant soils by Yu and Houlsby (1991) was developed assuming isotropic stress field conditions, i.e., the coefficient of lateral earth pressure at rest, K_o=1.0. As mentioned earlier, such assumption may be justifiable for some applications such as the interpretation of pressuremeter tests and evaluation of shaft capacity of tapered piles. However, this

assumption is not justifiable for HDD application and may introduce an error more than 50% due to the K_o effect alone (apart from the C/D effect). In order to account for this effect, a correction factor was obtained utilizing a nonlinear regression analysis of the results obtained from the parametric study. The results were obtained for seven different values of coefficient of lateral earth pressure at rest, K_o (1.0, 0.9, 0.8, 0.7, 0.6, 0.5 and 0.4). The proposed correction factor depends on the coefficient of lateral earth pressure at rest, Ko; the cover to depth ratio, C/D; and the ratio of the current radius to the original radius, a/ao, as shown in the following formula.

$$R_k = (K_o - 1)(0.5 - \frac{1.08}{C/D} + \frac{0.57}{a/a_o}) - 0.24(K_o^2 - 1) \qquad [17]$$

R_k should be added to the coefficient R_d to get an overall correction factor that accounts for both the coefficient of lateral earth pressure at rest and the embedment depth.

8 CORRECTION FOR THE COUPLED EFFECT OF THE EMBEDMENT DEPTH AND IN-SITU STRESS ANISOTROPY

It is common that an HDD installation encounters soil conditions that involve both initial stress anisotropy and low burial depth. For example, pipes with diameters ranging from 300mm to 600 mm installed just blow the frost depth of around 2 to 3 meters would result in an embedment depth ratio (C/D) ranging from 5 to 10. These shallow C/D ratios alone can result in more than 40% overestimation. Coupling this with the effect of initial stress anisotropy, the overestimation can reach 90% or more, i.e. nearly double the cavity pressure value. This vast overestimation can have significant impact on the selection of

the equipment needed for the installation, which may adversely impact the economic feasibility of the project.

8.1 Procedure for calculating cavity expansion pressure

A procedure is proposed herein to correct the predictions of the CFS accounting for the coupled effects of initial stress anisotropy and free surface, as follows:

i) Calculate the initial stress P_o, which corresponds to the initial cavity with radius a_o.

ii) Calculate the parameters given by Equations 1 o 9, which are functions of soil properties.

iii) For a given value of the additional cavity pressure, P, less than $P_1 = (\alpha - 1)P_o/(\alpha + 1)$, the response remains in the elastic stage of expansion and the corresponding radius a can be calculated by Equation 10.

iv) For an additional cavity pressure, P, exceeding the limiting pressure P_1, the cavity pressure ratio R is calculated from Equation 13.

v) Equations 14 and 15 are used to evaluate A_1 – only a few terms are sufficient.

vi) Evaluate a/a_o from Equation 12, and from that the cavity pressure can be determined.

vii) For the cases with initial isotropic stress, i.e. K_o=1, the calculated cavity pressure ratio is corrected to account for the burial depth using the correction factor, R_d, given by Equation 16, viz:

$$\left(\frac{P_t}{P_o}\right)_{\text{Corrected}} = \left(\frac{P_t}{P_o}\right)_{\text{CFS}} \times R_d$$

viii) For cases involving initial stress anisotropy, i.e. K_o<1, the ocalculated cavity pressure ratio is corrected to account for both stress anisotropy and burial depth using the

the correction factor, R_{dk}, which is the summation of the two correction factors, R_d and R_k, i.e.,

$$\left(\frac{P_t}{P_o}\right)_{Corrected} = \left(\frac{P_t}{P_o}\right)_{CFS} \times R_{dk}$$

where,

$$R_{dk} = R_d + R_k$$

8.2 Evaluation of the proposed procedure

8.2.1 Soil strength characterization

The shear strength of sand depends on a number of factors, including the nature of loading (triaxial or plane strain), drainage conditions (drained or undrained), initial state (loose or dense), and the type of fabric (fine or coarse). The angle of dilatancy, ψ, of sand is affected by the relative density and the effective stress (Bolton, 1986). Depending on the sand mineralogy (quartz or feldspar), typical values of the angle of internal frication of sands range from 30º to 40º, whereas the typical values of ψ range from 0º to 15º.

8.2.2 Results of the evaluation process

The applicability of the proposed correction procedure was evaluated for several cases covering a practical range of soils, ranging from loose to dense sand; geometric parameters ranging from C/D = 2.5 to 20; and initial stress anisotropy with K_o ranging from 0.4 to 0.8. Table 2 summarizes the geometric information and soil properties of the considered cases.

Figure 14 presents some of the corrected cases for low embedment ratios (i.e., C/D = 2.5 and 5). The results of the CFS adjusted using the correction factors are within 7% of the FE calculations. Thus, the proposed correction factor reduces the difference between the CFS and the FE from up to 86% to less than 7%. Figure 15 presents some of the corrected results for medium and high embedment ratios (i.e., C/D = 10 and 20). The corrected CFS results are within less than 9% of that of the FE calculations.

9 CONCLUSIONS

The results obtained in this study demonstrated that the closed form solution for cavity expansion due to Yu and Houlsby (1991) can be used reliably for cases subjected to an initial isotropic stress and embedment depth, C/D = 20 or higher. However, as the embedment depth decreases, the free surface condition affects its accuracy. The study also showed that the stress anisotropy conditions can lead to a significant overestimation of the cavity pressure calculated from the closed form solution. This overestimation can have significant implications when evaluating the forces associated with HDD installations and sizing the required equipment for the operation. It is therefore necessary to correct the predicted pressure values to account for effects of embedment and stress anisotropy. An analytical procedure to account for the effects of embedment and/or stress anisotropy was proposed. The proposed procedure was evaluated against several cases covering a wide spectrum of soil properties and geometrical configurations. The results obtained using the proposed method confirmed its usefulness and its ability to estimate the cavity pressures within 10% of the values obtained using FEA calculations.

REFERENCES

Bishop, R.F., Hill, R. and Mott, N.F. 1945. Theory of indentation and hardness tests. Proc. Phys. Soc., 57: 147

Bolton, M.D. 1986. The strength and dilatancy of sands. *Geotechnique* 36(1): 65-78.

Carter, J.P., Booker, J.R. and Yeung, S.K. 1986. Cavity expansion in cohesive frictional soils. *Geotechnique* 36(3): 349-358

Chadwick, P. 1959. The quasi-static expansion of a spherical cavity in metals and ideal soils. Q. J. Mech. Appl. Math., 12: 52-71.

El Naggar, M.H. and Sakr, M. 2000. Evaluation of axial performance of tapered piles from centrifuge tests. Canadian Geotechnical Journal, 37(6): 1295-1308.

Fernando, V. and Moore, I.D. 2002. Use of cavity expansion theory to predict ground displacement during pipe bursting. Proc. of Pipelines 2002, ASCE, Cleveland, OH, July, 11pp

Gibson, R. E. & Anderson, W. F. 1961. In situ measurement of soil properties with the pressuremeter. Civil Engineering Public Works Rev. 56: 615-618.

Hill, R. 1950. The mathematical theory of plasticity. Oxford University Press, London.

Houlsby, G.T. and Withers, N.J. 1988. Analysis of the cone pressuremeter test in clay. *Geotechnique*, 38: 573-587.

Hughes, J. M. O., Wrath, C. P. & Windle, D.1977. Pressuremeter tests in sands. *Geotechnique*, 27(4): 455-477.

Palmer, A. C. (1972). Undrained plane-strain expansion of a cylindrical cavity in clay: a simple interpretation of the pressuremeter test. *Geotechnique* 22(3): 451-457.

Randolph, M. F., Carter, J. P. & Wrath, C. P.1979. Driven piles in clay--the effects of installation and subsequent consolidation. *Geotechnique* 29(4): 361-393.

Salgado, R., Mitchell, J.K., and Jamiolkowski, M. 1997. Cavity expansion and penetration resistance in sand. ASCE, Journal of Geotechnical and Geoenvironmental Engineering, 123(4): 344-354.

Vesic, A. S. 1972. Expansion of cavities in infinite soil mass. J. Soil Mech. Fdns Div. ASCE 98, SM3, 265-290.

Yu, H.S and Houlsby, G.T. 1991. Finite cavity expansion in dilatant soils: loading analysis. *Geotechnique*, Vol. 41:173-183.

Yu, H.S. and Houlsby, G.T. 1995. A large strain analytical solution for cavity contraction in dilatant soils. International Journal for Numerical and Analytical Methods in Geomechanics, Vol. 19:793-811.

Yu H.S. and Rowe R.K.1999, Plasticity solutions for soil behaviour around contracting cavities and tunnels. International Journal for Numerical and Analytical Methods in Geomechanics, Vol. 23: 1245-1279.

Yu H.S. and Carter, J.P. 2002. Rigorous similarity solutions for cavity expansion in cohesive-frictional soils. International Journal of Geomechanics, Vol. 2(3).

Table 1. Selected results of the parametric study.

C/D	Closed form Solution		Finite Element Analysis		Error %
	a/a_o	P/P_o	a/a_o	P/P_o	
2.5	1	0	1	0	0.00%
2.5	1.03	7.70	1.03	6.13	25.61%
2.5	1.06	10.30	1.06	8.44	22.08%
2.5	1.09	11.80	1.09	9.35	26.25%
2.5	1.20	15.17	1.20	11.12	36.48%
2.5	1.30	16.98	1.30	11.82	43.68%
2.5	1.40	18.20	1.40	12.66	43.72%
2.5	1.50	19.25	1.50	12.49	54.06%
5	1	0	1	0	0.00%
5	1.02	4.97	1.02	4.51	10.21%
5	1.06	7.62	1.06	6.48	17.64%
5	1.09	9.05	1.09	7.31	23.85%
5	1.20	11.57	1.20	8.92	29.69%
5	1.30	12.95	1.30	9.81	32.05%
5	1.40	13.92	1.40	10.15	37.18%
5	1.50	14.67	1.50	10.45	40.41%
7.5	1	0	1	0	0.00%
7.5	1.02	4.27	1.02	4.15	3.01%
7.5	1.05	5.97	1.05	5.60	6.62%
7.5	1.09	7.77	1.09	6.78	14.56%
7.5	1.20	9.87	1.20	7.89	25.16%
7.5	1.30	11.07	1.30	8.69	27.37%
7.5	1.40	11.90	1.40	9.05	31.43%
7.5	1.50	12.50	1.50	9.61	30.06%
10	1	0	1	0.000	0.00%
10	1.01	3.45	1.01	3.40	1.48%
10	1.04	5.37	1.04	5.09	5.47%
10	1.09	6.88	1.09	6.46	6.43%
10	1.20	8.80	1.20	7.39	19.03%
10	1.30	9.90	1.30	8.23	20.22%
10	1.40	10.65	1.40	8.66	23.04%
10	1.50	11.19	1.50	8.88	26.06%
20	1	0.00	1	0.000	0.00%
20	1.02	2.97	1.02	2.89	2.63%
20	1.03	3.77	1.03	3.73	0.94%
20	1.09	5.28	1.09	5.26	0.43%
20	1.20	6.74	1.20	6.65	1.34%
20	1.30	7.55	1.30	7.39	2.16%
20	1.40	8.07	1.40	7.93	1.72%
20	1.50	8.47	1.50	8.22	3.09%

Table 2: geometric information and soil properties of the considered cases

Case #	C/D	Soil Properties					Max. Error %	
		K_o	ϕ^o	ψ^o	υ	*E (MPa)*	***Before Correction***	***After Correction***
1	2.5	0.4	40	15	0.4	90	76.34%	6.08%
2	2.5	0.4	40	0	0.4	90	76.42%	6.17%
3	5	0.4	40	0	0.4	60	86.21%	4.02%
4	5	0.5	35	0	0.3	20	69.17%	2.26%
5	7.5	0.5	33	10	0.3	60	61.11%	1.69%
6	7.5	0.66	38	10	0.3	90	52.06%	6.87%
7	10	0.8	30	15	0.35	20	27.36%	1.95%
8	10	0.8	30	0	0.35	20	24.03%	1.88%
9	10	0.8	40	15	0.35	80	37.66%	8.95%
10	10	0.8	40	0	0.35	80	41.64%	9.5%
11	20	0.6	35	10	0.35	40	34.32%	1.72%
12	20	0.6	35	0	0.35	40	42.41%	8.32%

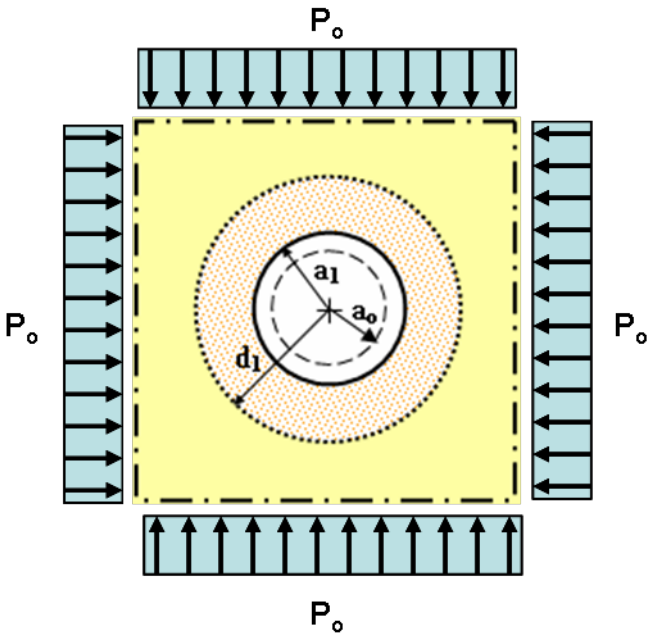

Figure 1. Geometry of the expansion phase.

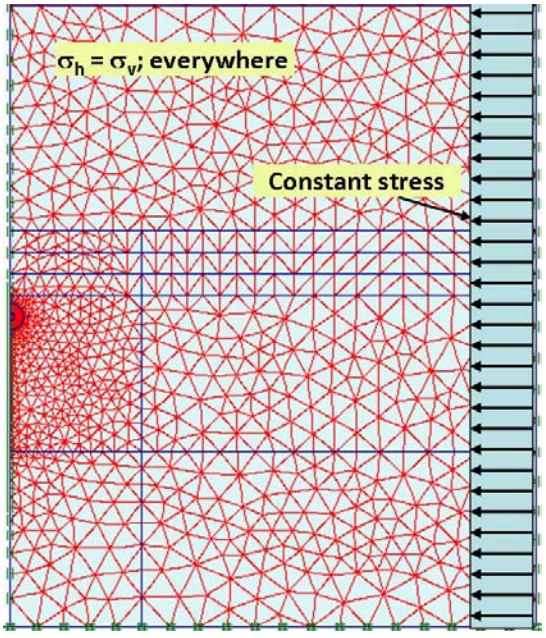

Figure 2. Problem geometry and the FE Mesh 1

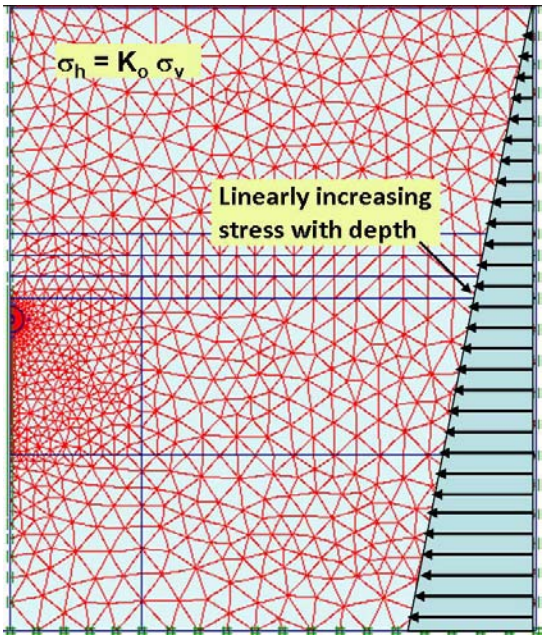

Figure 3. Problem geometry and the FE Mesh 2

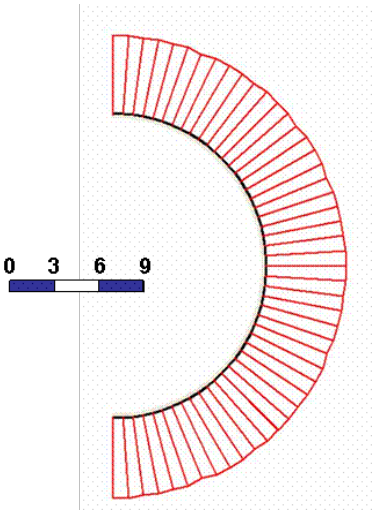

Figure 4. Radial cavity pressure normalized by initial soil pressure, P/Po

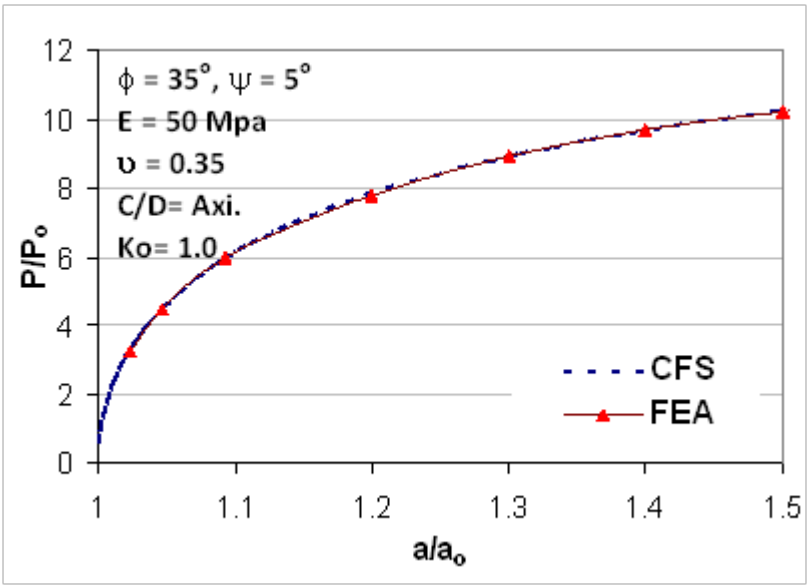

Figure 5. Radial cavity pressure normalized by initial soil pressure, P/Po, versus the cavity radius normalized by the initial cavity radius, a/ao, for medium sand.

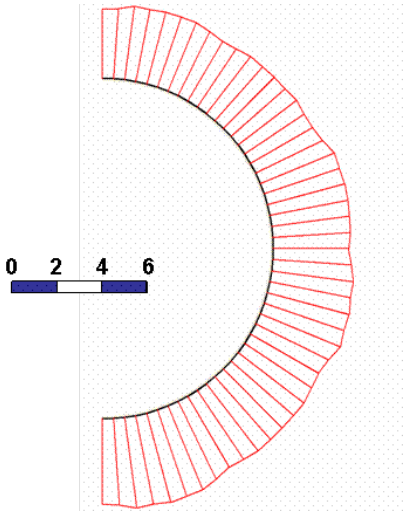

Figure 6. Radial cavity pressure normalized by initial soil pressure, P/Po

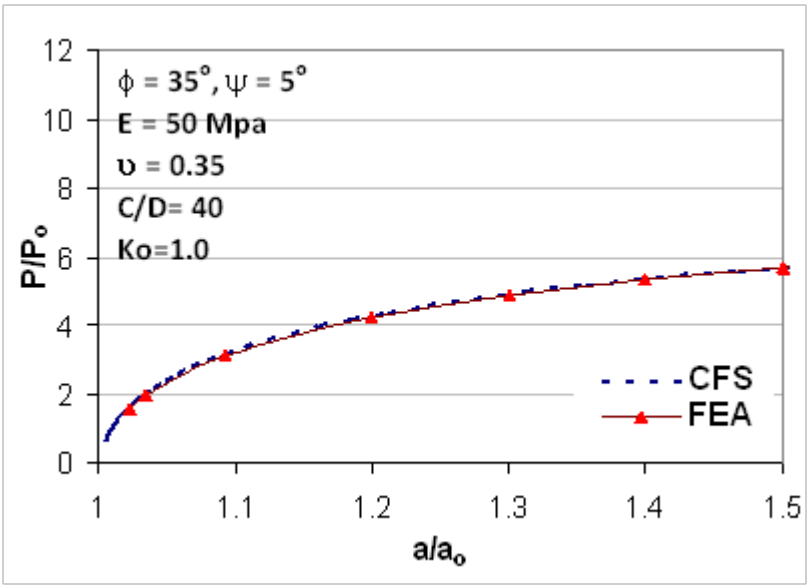

Figure 7. Radial cavity pressure normalized by initial soil pressure, P/P_o, versus the cavity radius normalized by the initial cavity radius, a/a_o, for C/D=40.

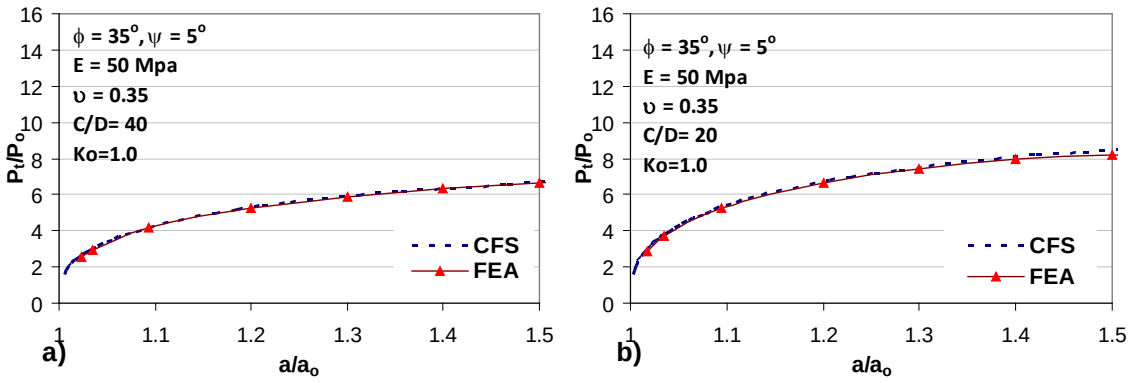

Figure 8. Radial cavity pressure normalized by initial soil pressure, P/Po, versus the cavity radius normalized by the initial cavity radius, a/ao, for: a) C/D=40, b) C/D=20.

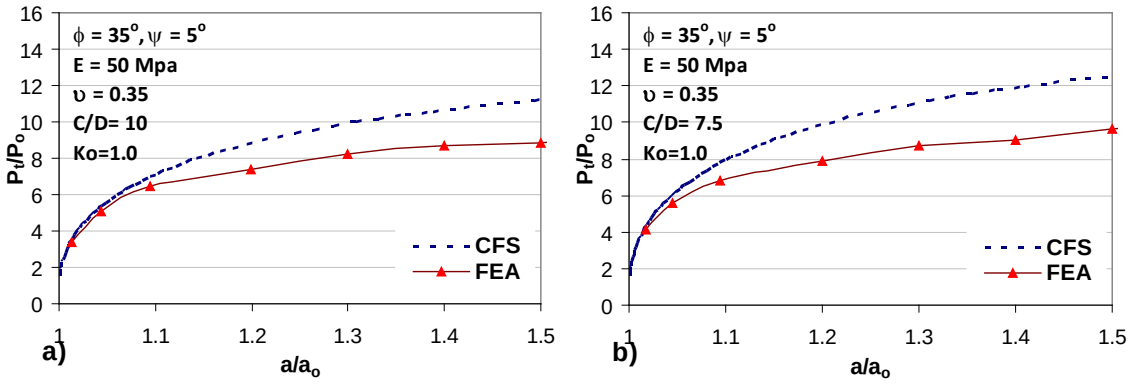

Figure 9. Radial cavity pressure normalized by initial soil pressure, P/Po, versus the cavity radius normalized by the initial cavity radius, a/ao, for: a) C/D=10, b) C/D=7.5.

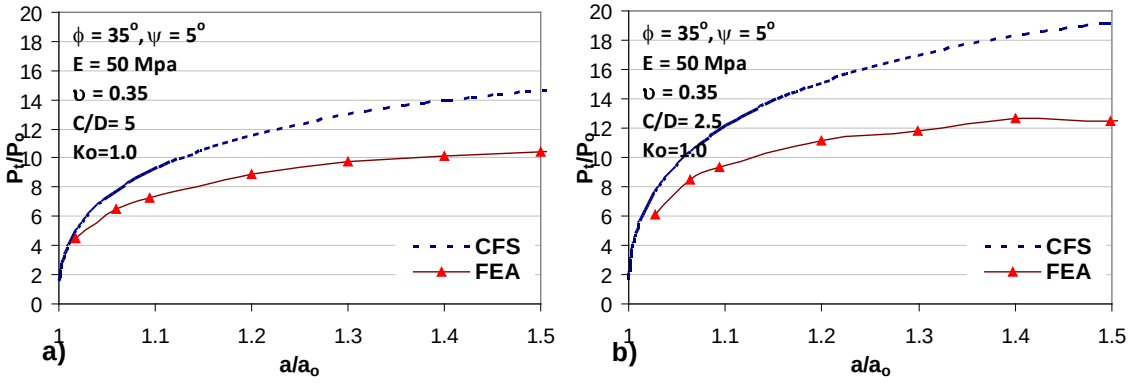

Figure 10. Radial cavity pressure normalized by initial soil pressure, P/Po, versus the cavity radius normalized by the initial cavity radius, a/ao, for: a) C/D=5, b) C/D=2.5.

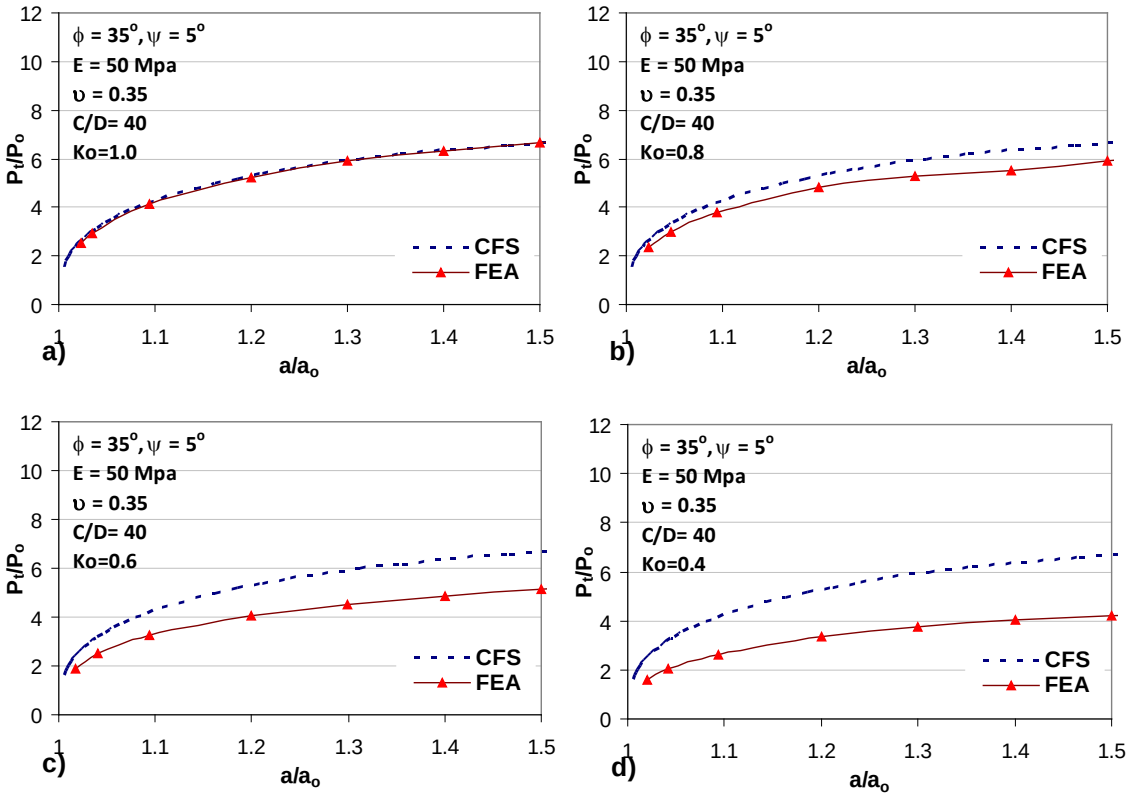

Figure 11. Radial cavity pressure normalized by initial soil pressure, P/Po, versus the cavity radius normalized by the initial cavity radius, a/ao, for: a)Ko =1.0, b) Ko =0.8, c) Ko =0.6, d) Ko =0.4.

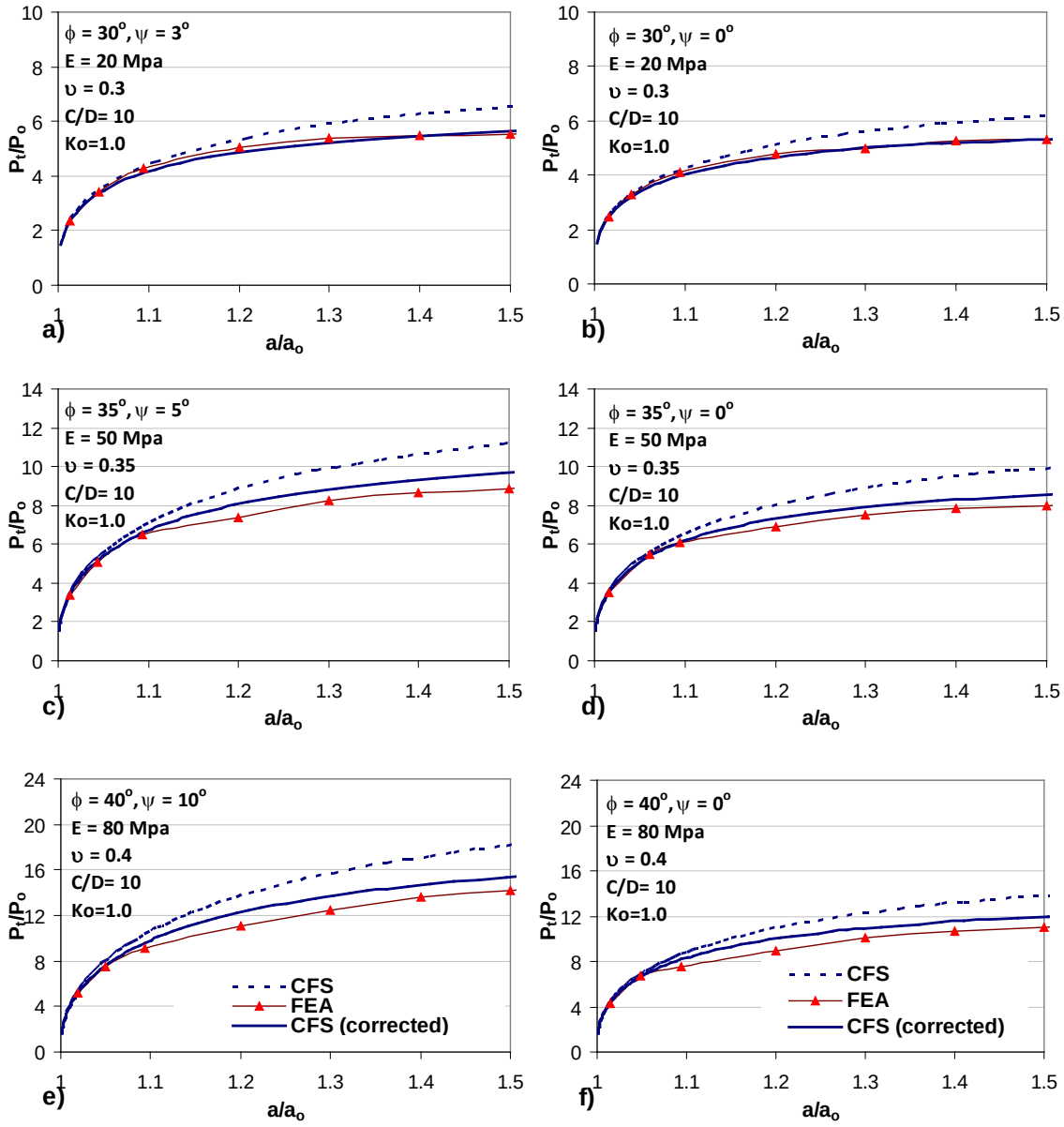

Figure 12. Radial cavity pressure normalized by initial soil pressure, P/Po, versus the cavity radius normalized by the initial cavity radius, a/ao, for sample of some corrected cases for C/D=10 and Ko=1.0.

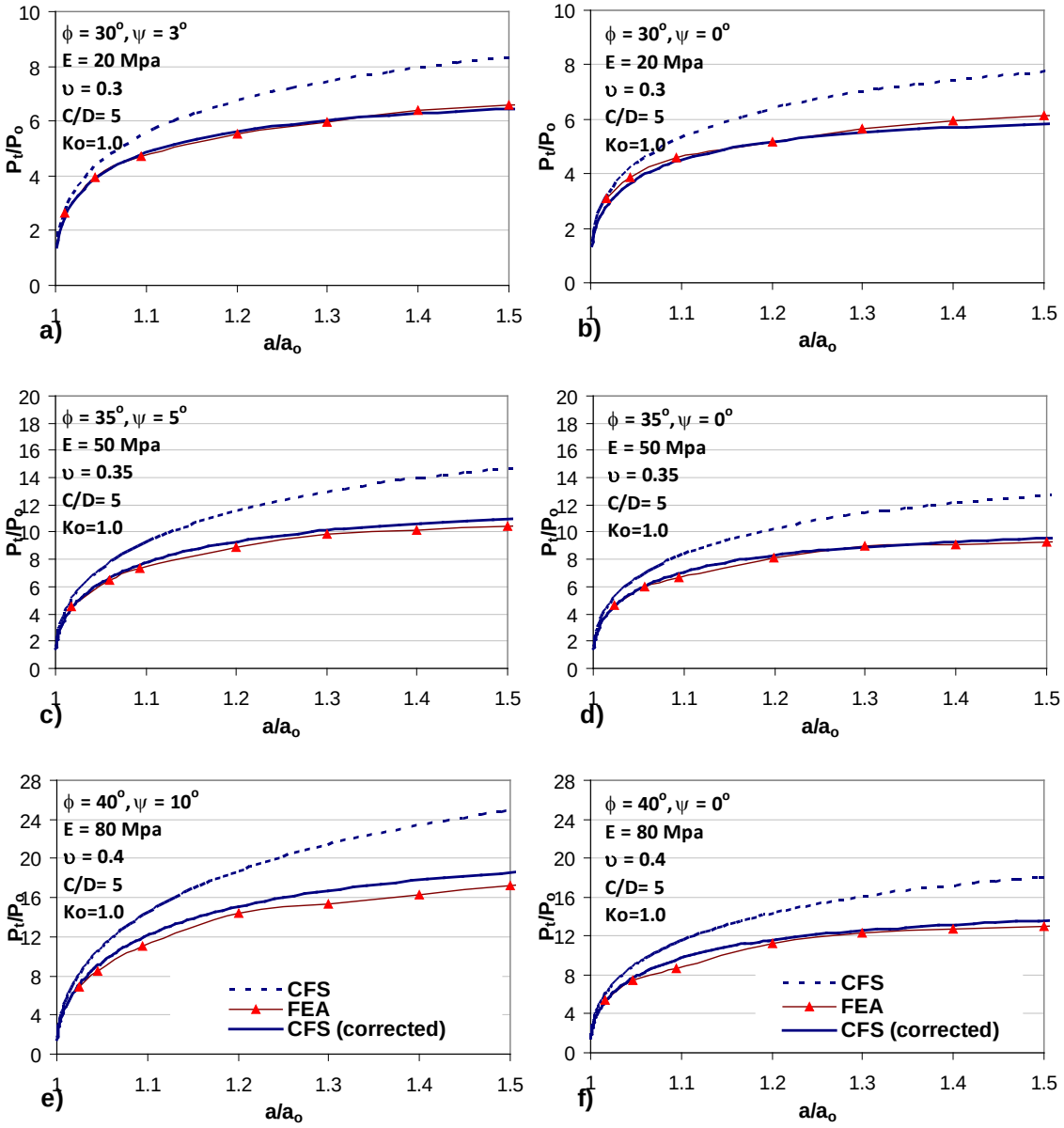

Figure 13. Radial cavity pressure normalized by initial soil pressure, P/Po, versus the cavity radius normalized by the initial cavity radius, a/ao, for sample of some corrected cases for C/D=5 and Ko=1.0.

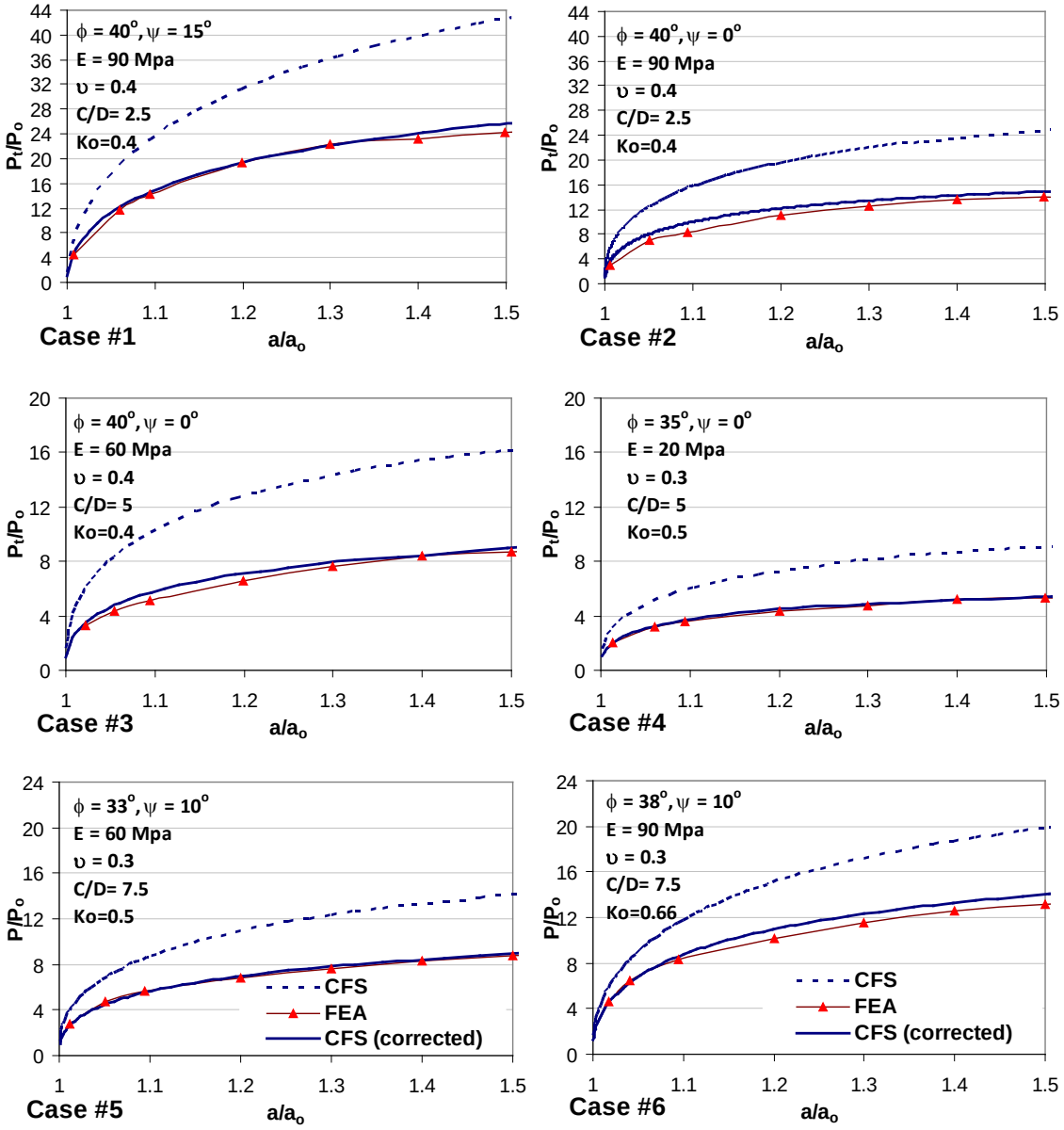

Figure 14. Radial cavity pressure normalized by initial soil pressure, P/Po, versus the cavity radius normalized by the initial cavity radius, a/ao, for sample of some corrected cases for combined effect of C/D and K_o low embedment.

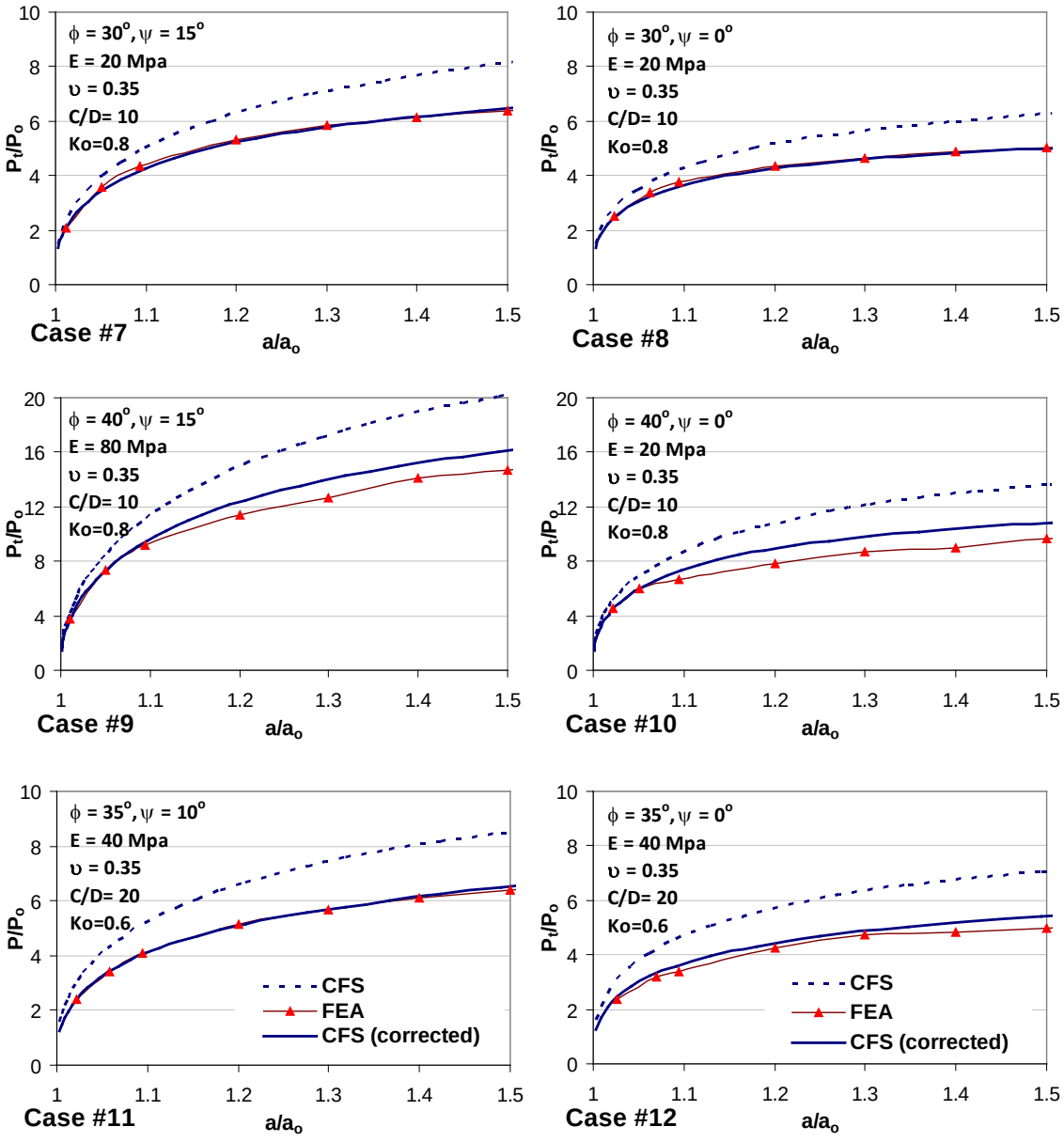

Figure 15. Radial cavity pressure normalized by initial soil pressure, P/Po, versus the cavity radius normalized by the initial cavity radius, a/ao, for sample of some corrected cases for combined effect of C/D and K_o medium and embedment.